2016

On the Aerodynamic Properties of Slotted-Flap Flow-Control Devices for Wind Turbine Applications

Muraleekrishnan Menon Menon Muraleedharan Nair
Michigan Technological University, mmenon@mtu.edu

ON THE AERODYNAMIC PROPERTIES OF SLOTTED-FLAP FLOW-CONTROL DEVICES FOR WIND TURBINE APPLICATIONS

By

Muraleekrishnan M. Menon

A THESIS

Submitted in partial fulfillment of the requirements for the degree of

MASTER OF SCIENCE

In Mechanical Engineering

MICHIGAN TECHNOLOGICAL UNIVERSITY

2016

This thesis has been approved in partial fulfillment of the requirements for the Degree of MASTER OF SCIENCE in Mechanical Engineering.

Department of Mechanical Engineering - Engineering Mechanics

Thesis Advisor: *Dr. Fernando L. Ponta*

Committee Member: *Dr. Lucia Gauchia*

Committee Member: *Dr. Leonard J. Bohmann*

Department Chair: *Dr. William W. Predebon*

Dedication

To my brother, Krishnakumar M.

who has always been a great inspiration to pursue science

Contents

List of Figures

List of Tables

Acknowledgments

It is indeed a great privilege to have worked under the guidance of Dr. Fernando L. Ponta for my master's research. He has been an excellent mentor in school, a great friend outside, and a remarkable source of inspiration for pursuing the path of research. I would like to place on record my sincere gratitude to him for serving as the academic adviser towards the completion of this degree. I am grateful to Dr. Lucia Gauchia, and Dr. Leonard J. Bohmann for their time and valuable inputs as members of the advisory committee.

I am grateful to the National Science Foundation for extending financial support towards conducting this valuable research in science, which serves as a partial fulfillment for my master's degree.

The technical brainstorming, casual conversations, and philosophical discussions in my research team has helped in shaping me into a better researcher. I am thankful to my research teammates for their continued support in this respect.

The immense support from my family, my girl friend, and my friends are the corner stones of motivation to do better everyday, and my gratitude towards them is hard to be expressed in words.

Nomenclature

h	Mesh size
ρ	Density
t	Time
x_i	First index in spatial reference frame
x_j	Second index in spatial reference frame
u_i	Velocity component in first index of spatial reference frame
u_j	Velocity component in second index of spatial reference frame
$\bar{u_i'}$	Mean fluctuating velocity component in first index of spatial reference frame
$\bar{u_j'}$	Mean fluctuating velocity component in second index of spatial reference frame
p	Static pressure
μ	Dynamic Viscosity
μ_t	Turbulent dynamic viscosity
τ_{ij}	Reynold's shear stress tensor
$\mathbf{S}_{ij}$	Mean strain rate tensor
k	Turbulent kinetic energy
ϵ	Turbulent dissipation rate
ω	Specific dissipation rate of turbulent kinetic energy
G_k	Generation of turbulent kinetic energy
G_ω	Generation of specific dissipation rate

Y_k	Dissipation of turbulent kinetic energy
Y_ω	Dissipation of specific dissipation rate
D_ω	Cross-diffusion term
S_k	User-defined source terms for turbulent kinetic energy, in $k-\omega$ formulation
S_ω	User-defined source terms for specific dissipation rate, in $k-\omega$ formulation
Γ_k	Effective diffusivity of turbulent kinetic energy
Γ_ω	Effective diffusivity of specific dissipation rate
Re	Reynold's Number
C_l	Coefficient of Lift
C_d	Coefficient of Drag
C_m	Coefficient of Pitching Moment
F_{lift}	Sectional lifting force
F_{drag}	Sectional dragging force
M_{aer}	Sectional pitching moment
c	Chord length of 2-D airfoil
v	Relative velocity of wind incident on the airfoil section
U_{rel}	Relative velocity of wind incident on the airfoil section
F_t	Sectional aerodynamic force in chord-wise direction
F_n	Sectional aerodynamic force in chord-normal direction
α	Angle of attack of wind
β	Angle of actuation of flap

List of Abbreviations

CFD	Computational Fluid Dynamics
DU	Delft University
FCD	Flow-control device
HAWT	Horizontal Axis Wind Turbine
MW	Mega-watt
NACA	National Advisory Committee for Aeronautics
NREL	National Renewable Energy Laboratory
RANS	Reynold's Averaged-Navier Stoke's
RWT	Reference Wind Turbine

Abstract

Wind energy is growing at a fast pace and utility-scale wind turbines growing in size with increasing rotor diameters. To sustain development of up-scaled wind turbines of tomorrow there is a need for innovation in load control methodologies. This thesis research targets an assessment of the aerodynamic properties of airfoil sections specifically intended for wind turbine applications, featuring them with flow-control devices. The use of fractional-chord trailing-edge flaps as slotted-flap devices on aerodynamically active parts of a turbine blade were studied. As modular devices attached externally on existing blade designs, they comfortably form a cost-effective means for active load control with low energy actuation. They also have advantages such as minimal design modifications to the original blade, relatively light-weight device, and lack of retooling of the manufacturing process.

The basis for an aerodynamic study was the NREL-5MW Reference Wind Turbine, which is a well-studied benchmark for large utility-scale wind turbines of today. This dissertation presents numerical results for the aerodynamic properties of two modified airfoil sections used on the blades designed for this turbine, NACA 64_3-618 and DU 93-W-210. These airfoils in their original configuration are used on the aerodynamically active parts of many contemporary wind turbines. A new set of coefficients defining the aerodynamic characteristics of these airfoils equipped with a fractional-chord trailing-edge flap of Clark Y profile are presented here. Defining the effects of flaps on airfoil sections specifically intended for wind turbine applications will suffice as a repository of useful aerodynamic data for a wider research community to develop new blade designs and load mitigation approaches for wind turbine rotors.

Chapter 1

Introduction

Wind is a major source of renewable, clean, and sustainable energy today and is growing at a fast pace. With the increasing energy needs, wind power is gaining more prominence in utility-scale power generation. The increasing penetration of wind power puts more emphasis on the predictability of power production and hence, the need to design aerodynamically reliable turbine blades for the future is becoming more significant. Utility-scale wind turbines of today consist of large three-bladed horizontal axis wind turbines (HAWT) operating within rated speeds of wind and are capable of producing anywhere between a few hundreds of kilowatts to as high as a few megawatts. Concept studies of state-of-the-art machines having huge blades 62 m in length promise production of up to 6 MW [5]. Other prototype studies of huge turbines such as the V164-8.0 MW manufactured by market leaders such as the Vestas show potential of producing up to 8 MW using blades as long as 80 m [6]. Studies conducted by Fichaux et al. [1] as part of the UpWind Project undertaken by European Wind Energy Association on huge offshore turbines indicate the capability to generate 20 MW with rotor diameters of 250 m. These are key indicators

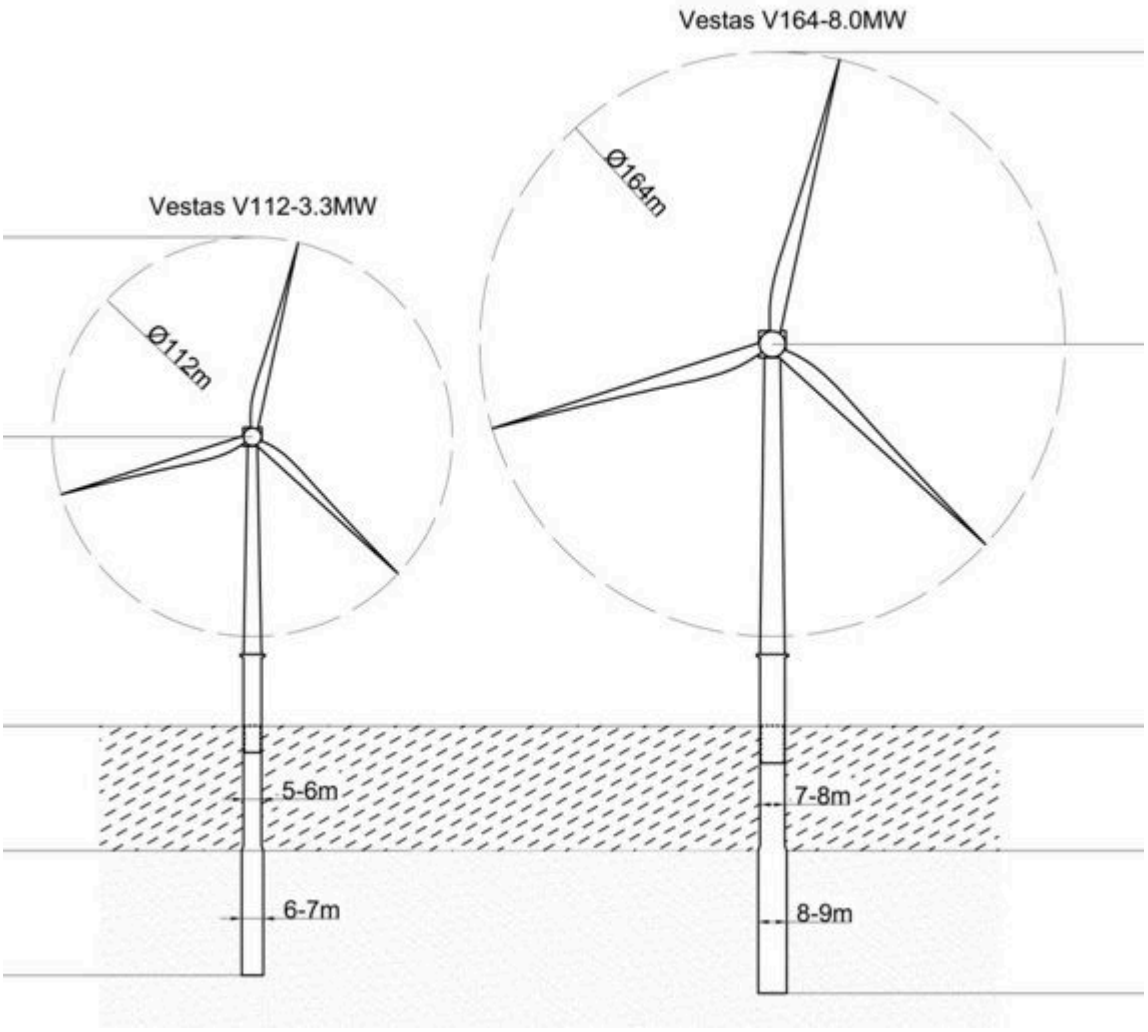

Figure 1.1: Schematics of two operational wind turbines manufactured by Vestas illustrates the scale of wind turbines and puts the rated power in perspective of rotor diameter.

of the trend in today's wind power industry to upscale the turbine rotor for higher power production.

HAWT are specifically designed machines capable of converting the kinetic energy in blowing wind to electrical energy in a multi-stage energy transformation. The key dynamics involved in these machines are the aerodynamics of the turbine rotor (which is

primarily the effect of blade design), control dynamics of interaction between the rotor and the control system, structural dynamics arising from the deformation of components due to prolonged exposure to dynamics loads, and the drivetrain dynamics that play a key role in transmitting the mechanical energy of the rotor to electrical energy produced by the generator. Longer blades ensure more swept area for the turbine rotor resulting in higher energy production, as the power generated increases linearly with the square of rotor diameter. The current trend in the utility-scale wind power industry is targeting a reduction in the cost of energy through this economies of scale factor. Hence, reducing the cost of energy involves larger rotors on turbines, resulting in the use of longer turbine blades to increase the swept area. A depiction of two operational wind turbines - V112 and V164 - manufactured by Vestas is shown in figure 1.1 to put in perspective how the size of wind turbine rotors are related to their rated power. This inclination in the industry to increase rotor size for more power has prevailed for a few decades and recent observations (as shown in the figure 1.2) suggest the definitive direction for the future. Turbines of tomorrow are expected to grow taller and larger in size, which essentially means the use of longer blades.

The proportional increase in power production associated with a linear increase in rotor diameter comes with a cubical increase in the weight, as defined by the *square-cubed law* [7]. Though this implies significant increase in rotor loads, due to the economies of scale factor, the cost of energy will still benefit from the use of larger rotors. The direct result of this scenario is increase significance of studies related to designing the right control mechanisms for the rotors [8]. Future machines need more attention to the blades and control strategies, especially as they play a key role in vibration loads, fatigue loads, and structural stability. Research revolving around innovative blade designs, wind-rotor interaction, and mitigation of aerodynamic rotor loads are widespread [9, 10, 11] and crucial for the

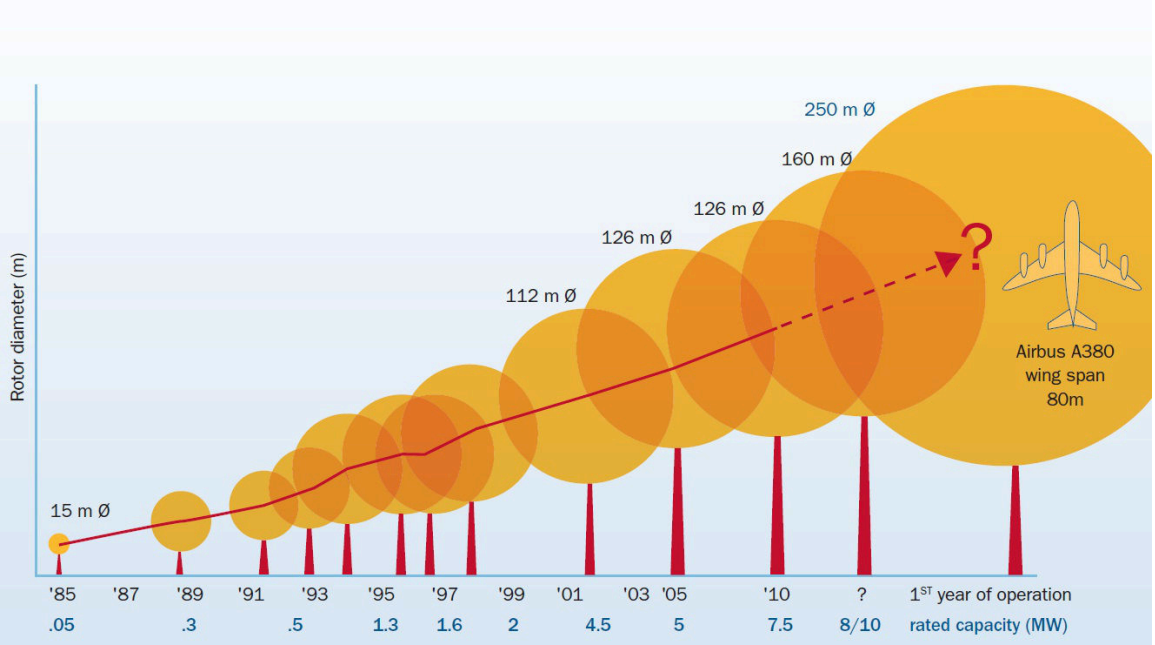

Figure 1.2: Illustration of progressive trend towards cost reduction through economies of scale factor, producing more power with the use of larger turbine rotors. Figure reproduced from UpWind project report by Fichaux et al. [1], © European Wind Energy Association. (See Appendix A for proof that this material is in the public domain for reuse).

growth of wind power industry. However, with an increased interest in this field of study National Renewable Energy Laboratories felt the necessity to establish a benchmark for future studies on large wind turbines. A conceptual model of a contemporary multi-megawatt utility-scale turbine was conceived as the "NREL offshore 5 MW baseline wind turbine" and is also commonly know as the NREL-5MW Reference Wind Turbine (RWT). This is a conventional three-bladed upwind variable-speed variable-pitch-controlled turbine, which indicates capability of the turbine blades to operate in variable rotational speeds and control capabilities by varying the pitch angle of the blades. Table 1.1 is an outline of the operational parameters of this turbine, and is significant for the current study.

Table 1.1
NREL-5MW RWT operational parameters

Description	Value
Rating	5 MW
Rotor Orientation	Upwind
Configuration	3 blades
Rotor, hub diameter	126 m, 3 m
Hub Height	90 m
Rated wind speed	11.4 m/s
Rated rotor speed	12.1 rpm
Overhang	5 m
Rotor pre-cone	2.5°

1.1 Load mitigation approaches

Extensive study on wind turbine blades has led the way to various load control methodologies in use today [12]. Passive methods make use of inbuilt properties such as the geometry to control various loads acting on the turbine in an open-loop methodology. Whereas active approaches are based on a feedback-response mechanism that alter particular characteristics of the turbine to mitigate loads and/or improve quality of power generation. Some of the strategies currently being studied and implemented are stall control [13], pitch control, active stall control, and yaw control. On the other hand, active control techniques make use of sensors and actuators (a closed-loop approach) that alter the aerodynamic properties of the blade to adapt with changing wind speed. Pitch-controlled turbines are examples of active control machines[14, 15, 16]. Pitching is a mechanism by which the pitch angle of the blade is adjusted to modify the angle of relative wind. In pitch-controlled machines, the pitch angle of blades are modified at the hub to control the loads by lowering the angle of attack, known as feathering and hence reducing the aerodynamic loads acting on the blade sections. Such controls actuated by hydraulic or electric motor driven gear systems

also reduce extreme loads on the turbine as wind speed increases beyond the rated value. Individual pitch control on blades enable assigning different pitching angles for different blades[17, 18] providing more flexibility of operation. In passive machines, pitch angles can be modified through specific blade designs such as a combination of spring and screw assembly that makes use of the high centrifugal force at the tip of the blade. An interesting variation of this control mechanism is known as the active stall control which is essentially pitching the blade towards stall [19]. Though it has the advantage of a closed loop control, the uncertainties of stochastic loads in the stalled sections of the blade at high speed winds makes it less reliable. Another strategy less frequently used in utility scale turbines is Yaw control [20, 21] which makes use of the Yaw system primarily built-in on a turbine to turn the rotor in to the wind. The strategy used here is to direct the rotor away from the wind instead and hence limit the effective relative wind that can generate power which also restricts the aerodynamic loads.

Increasing blade lengths is a major hold-up in the industry due to the lack of scalability of load mitigation strategies discussed above. On stall controlled machines, the fatigue loads on the aerodynamically active section of the blade increases with stalling and mitigation of such loads on larger blades requires closer study of the materials and methods involved in blade design and construction. Active pitch control is preferred over stall control for next generation utility scale super wind turbines, but they demand high rates of pitching [22] to mitigate dynamic loads due to gusts and changing wind conditions. Continued use of full span pitch controls for future turbines would become difficult to manage with the upscaling of turbine rotors and the proportional increase in weight of the blades. Alternatively, designs with fractional pitching for only the aerodynamically active part of the blade are also being studied. Such designs too have disadvantages of higher bending loads on

hydraulic actuators and increased complexity of the control mechanisms. The large gyroscopic moments involved with turning rotors in Yaw control methods make it less popular for upscaled wind turbines as well. This lack of scalability of load mitigation methodologies hinders the increase in upscaling of wind turbine rotors. Today, a lot of research is underway to tackle this bottleneck to an effective control mechanism [23, 24, 25].

1.2 Future of load control

The up-scaling of turbine blades would benefit from a rationale change in load control strategy by incorporating either one or a combination of more than one of the innovative techniques such as variable-speed stall, flexo-torsional adaptive blades, and active flow-control devices. These cutting-edge techniques are being widely studied in the wind power industry and have the potential to shape the future of load control for wind turbines. There are essentially two genres of stall-controlled wind turbines - constant-speed and variable-speed, which functions as their names suggest. The former kind rotates at constant speed and as the wind speed increases, allows certain sections of the blade to operate in stall condition, which reduces the lift generated and hence the driving torque. Variable-speed stall machines on the other hand, combine aerodynamic characteristics of rotor blades and doubly-fed induction generation with power electronics to regulate torque, power, and reduce drive-train loads [7]. By controlling rotor speed, the turbines aim at increasing energy capture at low winds and hence maximizing power production while limiting power output to the rated value in high wind conditions. Such machines perform better than constant-speed stall machines to reduce the extreme loads on the rotor and drive train by employing what is known as “soft stall”. At high wind speeds, the blades still operate in stall but in

a more benign way [26]. However, the inertial loads acting on the rotor blades are still a major concern for up-scaling of these machines. Use of adaptive flexo-torsional blade designs that control loads using built-in bend-twist coupling characteristics are another alternative [27, 28, 29, 30]. As the turbine blades are very long and having only one point of arrest at the root, can be structurally treated as a complex one-dimensional cantilever beam that bends due to the loads acting during its operation. These innovative blades are internally designed to enable span sections to twist in a fashion that compensates for the bending caused by high wind loads. The variable twist of the blade span passively changes the angle of attack in certain sections and hence reduces the lift generated and high wind rotor loads. A realistically attainable optimum twist distribution would however restrict this coupling to the aerodynamically active span regions of the blade only. Another methodology proposes the use of active flow-control devices [23]. Flow-control devices (FCDs) are internal or external attachments that are capable of modifying the aerodynamic behavior of the entire blade. Primarily derived from aeronautic applications, where these devices were used to increase lift generated by modifying the camber and altering the flow around the airfoil, they are popularly known as high-lift devices. These devices also have fractional chord lengths with respect to the corresponding airfoil section chords [31], making it easier to handle in dynamic operating conditions. Modifying state-of-the art wind turbine blades through airfoil sections equipped with flow-control devices provide a great alternative in improved load control management for future super wind turbines.

1.3 Active flow-control devices for aerodynamic control

The airfoil sections used on the aerodynamically active parts of wind turbine blades are mostly derived from aeronautic applications and have a lot of similarity to those used on airplane wings [3] and helicopter rotor blades. Additionally, active FCDs such as fractional-chord flaps and ailerons have been extensively used in aeronautic applications and hence has the potential to impact the wind power industry in a similar manner. Sectional schematics of two types of flow-control devices are shown in figure 1.3. Flow-control devices can be widely classified as passive and active based on the scope of flow alterations and energy expenditure. Passive methods modify the flow without introducing external energy into the system but alters the flow through a mixing of high momentum and low momentum flow particles. This is achieved through techniques such as geometric modifications that manipulate the pressure gradient, fixed mechanical devices that control flow separation, or devices on the flow surface that help in drag reduction. Most times, these devices have fixed positions or geometrical orientations that are not controllable during regular operation. On the other hand, active devices used in flow control introduce auxiliary energy in to the flow field, and are designed to change their relative position during operation. These devices could either modify the flow without considering the state of flow or use a control loop that will implement the modification based on a measurement of the flow field using sensors. The control loop could either be feedforward or feedback, and in either case active control techniques have the advantage of being interactive and hence the ability to provide dynamic control actions based on inputs from the sensors. In a feedforward control loop, the controlled flow field parameter could be different from the measured flow field parameter as the flow progresses through the sensors and actuators. And in a feedback technique, there

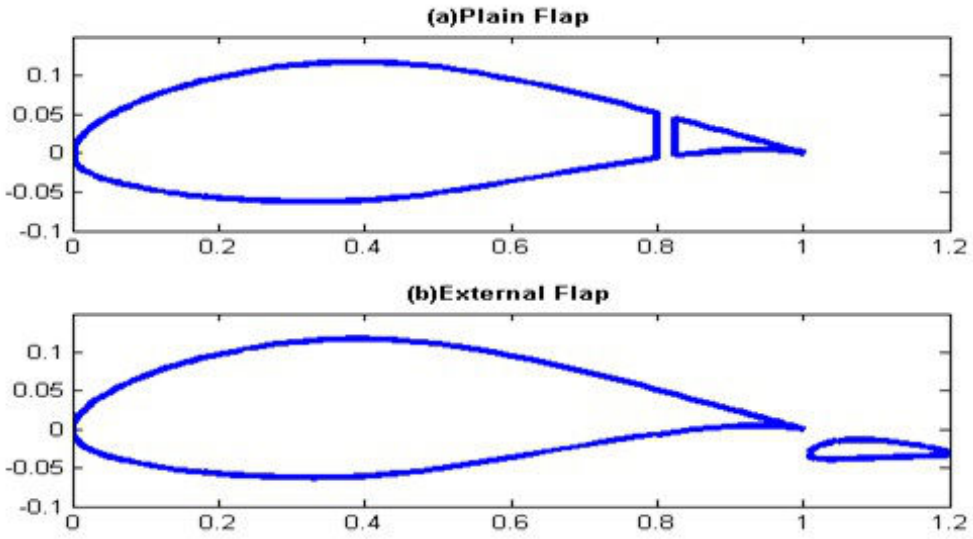

Figure 1.3: Examples of flow-control devices: (a) Plain Flap, (b) External Flap

are sensors downstream of the actuator which compares the controlled flow field parameter with reference to upstream measurements, and dynamically introduces energy at the actuator using predefined control laws. Active devices such as the slats attached near the nose of the wings and tail-end flaps have been in use on airplane wings as early as 1914 [32, 33]. Their use in aeronautical applications have become a commonplace and are now starting to gain grounds in wind power applications due to various inherent advantages. Some of the most common active FCDs used in wind turbine applications are microtabs, flexible trailing-edges, leading-edge slats, and trailing-edge flaps.

Mutli-element airfoils with two or three flaps are commonly used on airplane wings to modify the lift and drag characteristics during take-off and landing [34]. The technique of altering the aerodynamic behavior of airfoil sections through flow-control devices, specifically the use of a single element trailing-edge flap has considerable importance in wind

turbine applications. Early experimental studies by the National Advisory Committee for Aeronautics (N.A.C.A.) indicate that these flaps act as high-lift devices when used with aerodynamically active airfoils [2, 35, 36]. Span-wise location on the blade, relative position and orientation with the airfoil sections, and the profile of theses devices play significant roles in qualitative modification of the flow structures. As fractional-chord devices, they provide more ease of dynamic control and other advantages such as the lack of need to retool the existing manufacturing processes. Active control can be achieved based on a feedforward or feedback control loop guided by predefined algorithms that provide a range of operating conditions for the turbine rotor to adapt with the changing wind conditions. In this context, smart actuator systems studied by the European Rotorcraft Forum [37] encourage the use of dynamically controllable flaps on turbine blades. Numerical studies have also shown that multi-element airfoils used on inboard sections of wind turbine blades improve performance of the turbines in operating conditions [38]. Some of the benefits derived include lower cut-in wind speed, higher lift coefficients in low winds, better lift-to-drag ratio, and higher structural efficiency.

This dissertation focuses on a numerical assessment of active flow-control devices as a load control methodology through a study of airfoil sections specifically intended for wind turbine applications. As complicated aerodynamic structures undergoing cyclical rotation in dynamic wind conditions, analysis of wind turbine blades could be a tedious task. The combination of various factors such as fluctuating rotor loads, coupled aeroelastic behavior of turbine blades, interaction of blades with the tower, and dynamics of the control system adds more emphasis for a reliable assessment of the dynamics. With the increasing size of the rotors, these interlinking factors make wind-tunnel studies of next generation super turbines difficult, also considering the huge scaling factors involved in this process. Hence,

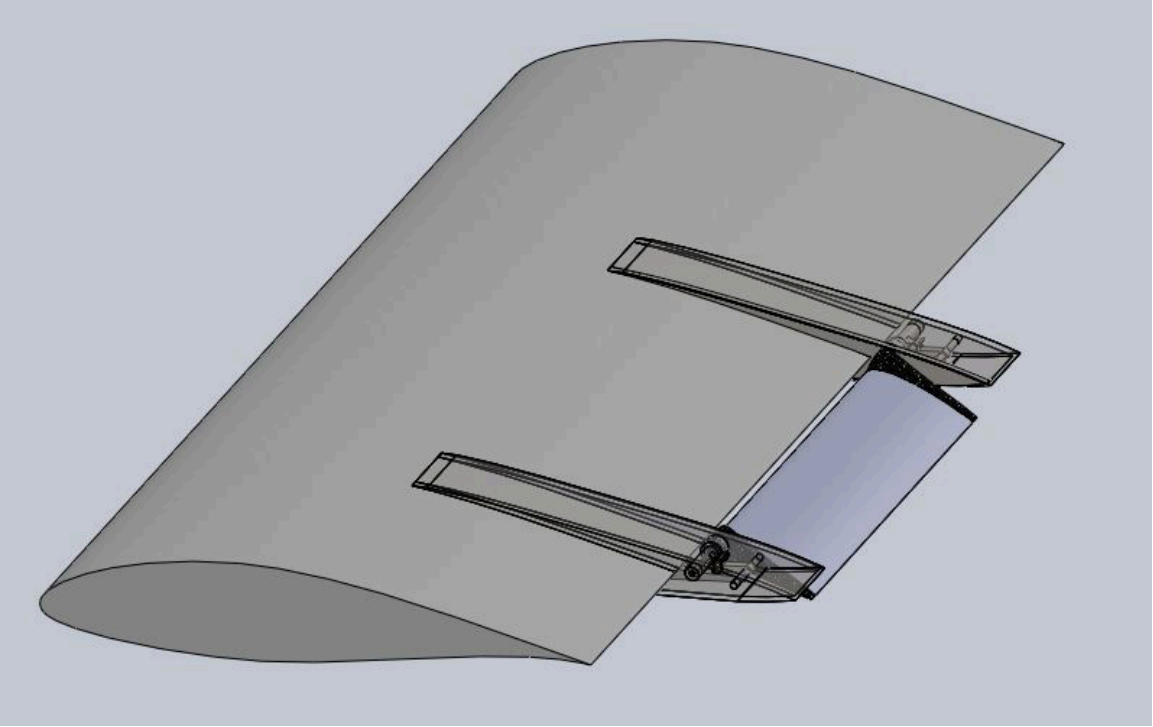

Figure 1.4: Schematic view of the trailing-edge flap and the modular attachment

studies should focus on full-scale analysis of turbine blades using efficient numerical models capable of taking these dynamics into consideration. And the starting point for this would be the determination of aerodynamic characteristics of airfoil sections equipped with trailing-edge flaps. External devices with fractional chord near the trailing edge of the main airfoil sections known as trailing-edge flaps are the specific target in this study [32, 39]. Based on the slotted trailing-edge flap concept, these modular devices could be appended to an existing blade design, providing a cost-effective way of active control with low energy actuation, and minimal modifications to the original blade design and manufacturing process. They can also be equipped with low-energy actuators to enable dynamic alteration of the flap orientation to suit a range of operating conditions. The numerical computations were carried out using a two-dimensional pressure-based Navier Stokes equation solver, ANSYS Fluent. The numerical model is standardized through a study of a NACA 23012

with a trailing-edge flap of Clark Y profile, which is a classical well-studied example of a multi-element airfoil-flap assembly used in aeronautical applications. New aerodynamic information is computed for NACA 64_3-618 and DU 93-W-210, which are typical airfoil sections used in wind turbine blade applications. In their original configuration, they are currently used on the NREL-5MW RWT [40], which could be regarded as a well-known benchmark case. There is currently no information available about their aerodynamic behavior in airfoil-flap assemblies and generating this information is the primary objective of the current study. Results from this study will provides useful information to add knowledge about the effects of trailing-edge flaps applied to airfoil sections specifically designed for wind turbine applications and forms a platform for developing new designs and load mitigation strategies for wind turbine rotors.

Chapter 2

Methodology

The first step towards implementing flow-control devices as a load control technique is developing modified airfoil sections, equipped with these trailing-edge flaps and computing their aerodynamic characteristics. Presence and activation of these devices will alter the properties of specific airfoil sections which in turn affect the operation of the entire turbine blade. Computation of the aerodynamic characteristics airfoil sections involves the determination of coefficients of lift, drag, and momentum for various flow conditions they could be subjected to during the operation of wind turbines. The range of conditions relevant to wind turbine operation is gauged as a range of angles of attack, essentially defining the regime of flow around the airfoil section. The aerodynamic coefficients vary with varying flow conditions, which is primarily based on the angle of wind (or attack) and is a key indicator to an aerodynamic assessment of any airfoil section. The aerodynamic coefficient for airfoils with and without FCDs were computed through a numerical model designed with a commercial Computational Fluid Dynamics (CFD) solver - ANSYS Fluent, which uses a Reynold's averaged Navier-Stokes equations approach based on the Finite-volume

discretization method. To ensure consistency of the computations, a systematized numerical procedure was developed through the validation of numerical results with experimental findings. Platt [2] published the results of experimental study conducted by the N.A.C.A. on high-lift devices such as airfoils with cambered trailing-edge flaps. Abbott and Doenhoff [3] consolidated aerodynamic coefficients for airfoil sections as graphical plots from various reports published by the N.A.C.A., which establishes the aerodynamic characteristics in their original configuration. The information taken from these two sources for a specific range of angles of attack, served as the experimental baseline in establishing the numerical procedure for the study of airfoils with and without flow-control devices.

Computational Fluid Dynamic(CFD) solvers are useful tools for conducting two dimensional airfoil section analyses to obtain the aerodynamic coefficients. Simulation using a CFD solver can be complicated in view of the various physical phenomena involved in the flow around an airfoil. The solver should have the ability to capture complicated fluid-structure interactions at various angles of attack, for changing geometry, near prominent flow regions, and for varying configurations of multi-element airfoils. Depending on the airfoil shape and relative position of the flap, the flow characteristics at the trailing edge could be complicated with boundary layer thickening, separated flow, reattachment of boundary layer, and vortex shedding. Especially, when the airfoil is near stall regime, it is more difficult to approximate the characteristics due to the dynamics of the flow [2]. Key factors for a reliable numerical model in the CFD analysis of two-dimensional airfoil sections are mesh design and selection of the turbulence model.

2.1 Mesh design

The computational domain formed by an assembly of discrete spatial elements forms the grid or the mesh. In the case of a time-dependent solution, there will be discretization on an additional domain in time. Discretization error, also commonly known as numerical error, results from the mismatch in representation of the governing equations of flow as algebraic expressions in the discrete space domain. The goal in developing an efficient numerical model is to reduce this error, which starts with designing an appropriate mesh. And in this respect, quality of the spatial grid is the most important aspect of the numerical analysis prior to the simulation. Numerical problems in this study involves development of steady-state solutions to two-dimensional airfoil sections and hence will need to deal with only the spatial domain.

Numerical computations are highly dependent on properties of the grid space especially the quality of the mesh, which is primarily a result of the mesh element size and number of computational nodes. As long as the definition of the problem is correctly done, the solution should approach continuity as the mesh size (h) approaches zero, which mostly also means higher number of meshing nodes. A prevailing issue in numerical computations is assessing the grid resolution, which often depends on the design geometry and flow conditions among other factors. However, a systematically refined grid should result in a continuum solution as the mesh size approaches zero, which can be considered as the true numerical solution. This is the closest solution to the exact representation of the governing equations, barring computer rounding off and truncation errors. As the mesh is refined,

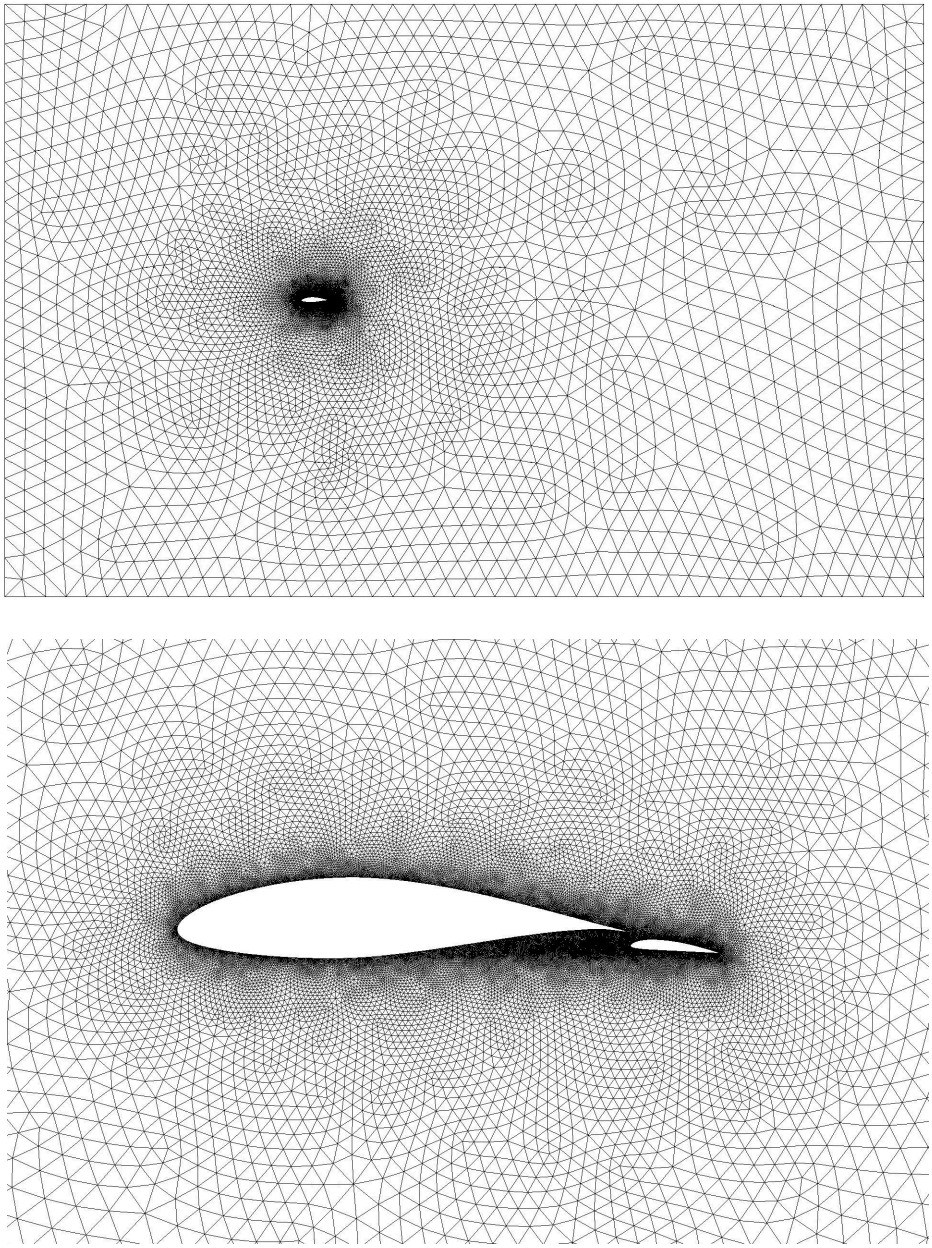

Figure 2.1: Initial mesh designed for Computation Fluid Dynamic analysis of NACA 64_3-618 with Clark Y profile trailing-edge flap. Top panel: global view of the grid space before initiating adaptive mesh refinement, bottom panel: closer view of the initial mesh. Notice denser mesh near the airfoil surface with elements growing in size towards the far-field boundary.

it can be observed that the solution becomes less sensitive to the mesh sizing and asymptotically approaches the continuum solution. An approach using two or more meshes in a consistent evaluation towards obtaining this asymptotic solution is called *mesh independence study* or *grid independence study*. It is based on the evaluation of one key indicator or more, which in most cases are flow properties of considerable significance. Conducting such a study is important in separating the dependency of a numerical solution from the properties of the discrete computational grid used.

It must be noted that CFD simulations are highly complicated and largely depend on the spatial discretization of the computational grid. To resolve physical behaviors such as gradient boundary layers, flow separation, and recirculation, it is necessary to follow a systematic approach and establish grid independence of the solution. The evaluation of two-dimensional airfoil sections involve external flows around the airfoil and hence, the computational grid is a region surrounding the airfoil profile. The grid should be designed with ample attention to key aspects such as node density, grid resolution, aspect ratio, element stretching, and orthogonality. Computations using grids with poor quality or extremely coarse distribution of nodes could trigger the propagation of numerical errors, eventually resulting in converged solutions that are far-off from true ones. Spacing of the wall boundaries is another important aspect of grid design in external flows, and should be done carefully to both avoid domain truncation errors and optimize the computational time. Figure 2.1 shows the computational grid designed for one of the test cases in this study, and is presented here as an example of a well designed mesh. The outer boundary walls are appreciably far from the airfoil surface as can be noticed in the top panel of the figure 2.1 and is depicted here to lay emphasis on the domain truncation effects that needs to be taken into consideration during mesh designing. It is also necessary to note the higher

mesh density closed to the airfoil surface where discretization of complex flow physics is most difficult.

The most important physical quantities in a two-dimensional airfoil analysis are coefficient of lift and coefficient of drag and form key indicators of some measure of grid convergence. Properties such as node distribution on airfoil surface and wall boundaries, mesh sizing, grid refinement ratio, and overall mesh density were varied to generate different meshes. A consistent numerical approach was adopted in evaluating each of the designed meshes to resolve for these coefficients in the range of angles of attack relevant for the study. The converged values of the coefficients and a standardized relative error (with respect to experimental values), for selected flow scenarios were used to establish the most optimum mesh design when the coefficients approached the asymptotic convergence. The result of this study was a consistent numerical grid with uniform mesh density, independent of mesh properties, and an optimized rate of convergence.

2.2 Turbulence modeling

Another important aspect in developing a reliable numerical model to assess two-dimensional airfoils is the modeling of turbulence, which becomes more crucial with a multi-element airfoil assembly. Selection of the turbulence model depends on various factors such as the accuracy of approximation needed, computational resources available, and standard practices in the field of study in addition to the primary task of representing the physics correctly. Numerically, fluid flows whether turbulent or not, are governed by a set

of dynamical partial differential equations representing the flow properties such as velocity and pressure. Turbulence is created by disturbances in a flow resulting in various flow features such as unsteady vortices and boundary layers that have varying length scales, which all interact with each other resulting in increased mixing and energy dissipation. Modeling such flow characteristics and estimating the effects of turbulence is called Turbulence Modeling. A common practice is to average the governing equations of the flow, focusing on large-scale, non-fluctuating aspects of the flow, but ensuring that the effects of small-scale disturbances are not ignored. Turbulence modeling approaches currently in use include Reynold's Averaged Navier-Stoke's, Large Eddy Simulation (LES), and Detached Eddy Simulation (DES). The approach that averages the Navier-Stoke's governing equations of flow by breaking down the flow quantities into a mean part and a fluctuating part, and then averaging them to obtain the governing equations for the mean flow is called Reynold's Averaged Navier-Stoke's (or RANS). The conservation of mass (equation 2.1) and momentum (equation 2.2) are represented in the RANS model as shown below:

$$\frac{\partial \rho}{\partial t} + \frac{\partial}{\partial x_i}\left(\rho\, u_i\right) = 0 \tag{2.1}$$

$$\frac{\partial}{\partial t}\left(\rho\, u_i\right) + \frac{\partial}{\partial x_j}\left(\rho\, u_i\, u_j\right) = -\frac{\partial p}{\partial x_i} + \frac{\partial}{\partial x_j}\left[\mu\left(\frac{\partial u_i}{\partial x_j} + \frac{\partial u_j}{\partial x_i} - \frac{2}{3}\,\delta_{ij}\,\frac{\partial u_l}{\partial x_l}\right)\right] + \frac{\partial}{\partial x_j}\left(-\rho\,\bar{u_i'}\,\bar{u_j'}\right) \tag{2.2}$$

where i and j represent the first and second index of a two-dimensional Cartesian spatial coordinate system, ρ is density of the fluid, t is time, μ is the dynamic viscosity, x_i, x_j represent the spatial reference frame in two dimension, u_i, u_j represent the velocities in

the respective spatial frames, $\bar{u_i'}$ and $\bar{u_j'}$ represent the mean of fluctuating velocity components, and p is the static pressure. These are essentially the same conservation equations as in Navier-Stoke's but the velocities and other variables represented in ensemble-averaged (time-averaged) form.

The key objective of RANS-based models is to solve for the Reynold's stresses. Such models are of interest to us and can be widely classified into Linear Eddy Viscosity, Non-liner Eddy Viscosity, and Reynold's Stress Transport models based on the methodology adopted in solving the Turbulence Closure Problem. Models that use the eddy viscosity approach, models the Reynold's stresses through linear/non-linear constitutive equations attempting to solve for the eddy viscosity. The third category uses a more complicated approach where the closure problem is solved in the second order and is mostly helpful in modeling highly complex flows. The linear eddy viscosity models are identified based on the additional equations employed to solve for the eddy viscosity, also commonly knows as the turbulent viscosity (μ_t). Most commonly used for engineering application, the two-equation linear eddy viscosity models are based on an approximation proposed by Boussinesq in 1887 [41]. This postulates a linear relation between the turbulent stresses (or Reynold's stress tensor, τ_{ij}) and the mean rate of shear (or mean strain rate tensor, $\mathbf{S}_{ij}$), as shown in equation 2.3 for an incompressible flow. The principal advantage of models using Boussinesq's approximation is the relatively low computational cost in computing the turbulent viscosity.

$$-\rho\bar{u_i'}\,\bar{u_j'} = \mu_t \left(\frac{\partial u_i}{\partial x_j} + \frac{\partial u_j}{\partial x_i}\right) - \frac{2}{3}\,\rho\,k\,\delta_{ij} \tag{2.3}$$

where μ_t is the scalar turbulent viscosity, k is the mean turbulent kinetic energy, and $\mathbf{S}_{ij} = \left(\frac{\partial u_i}{\partial x_j} + \frac{\partial u_j}{\partial x_i}\right)$ is the mean strain rate tensor. Also, $\tau_{ij} = -\rho\bar{u_i'}\bar{u_j'}$ is the representation of the Reynold's stresses, where ρ is the density of the fluid, and $\bar{u'}$ are the mean fluctuating velocity components of flow in spatial coordinates i and j.

As the name suggests, two-equation models have two additional transport equations to represent the turbulent properties of the flow and hence allows an evaluation of the history such as convection and diffusion of turbulent energy. One of these transported variables is almost always the turbulent kinetic energy k, and the second one could be either turbulent dissipation rate ϵ, or the specific dissipation rate ω, depending on the turbulence model chosen. Qualitatively, they signify the energy in the turbulent flow and the scale of turbulence. ANSYS Fluent provides a list of turbulence models to select from, which are based on the principles described above. The standard versions the k-ϵ and the k-ω and a few variations have become very popular in solving many engineering problems. The standard k-ϵ model was first introduced by Launder and Spalding [42], is based on model equations derived for turbulent kinetic energy (k), and the rate of dissipation (ϵ) and has proven to be an efficient approach in many practical engineering applications. This model assumes the flow to be fully turbulent and hence neglects the effects of molecular viscosity. The k-ω uses model equations for specific dissipation of turbulence (ω) instead and is an equally capable model in many flow scenarios [43]. This model uses two additional transport equations to solve the turbulent kinetic energy, k and specific dissipation rate, ω, as can be seen from equations 2.4 and 2.5. Using simple Dirichlet boundary conditions, this model keeps the approach simple while maintaining comparable accuracy, and hence is considered superior to other two-equation models in terms of the numerical stability. All two-equation models are efficient in solving the problem taking specific aspects of the flow into consideration,

but none of them are all-inclusive.

$$\frac{\partial}{\partial t}(\rho\, k) + \frac{\partial}{\partial x_i}(\rho\, k\, u_i) = \frac{\partial}{\partial x_j}\left(\Gamma_k \frac{\partial k}{\partial x_j}\right) + G_k - Y_k + S_k \tag{2.4}$$

$$\frac{\partial}{\partial t}(\rho\, \omega) + \frac{\partial}{\partial x_i}(\rho\, \omega\, u_i) = \frac{\partial}{\partial x_j}\left(\Gamma_\omega \frac{\partial \omega}{\partial x_j}\right) + G_\omega - Y_\omega + D_\omega + S_\omega \tag{2.5}$$

where Γ represents the effective diffusivity, G denotes the generation, Y denotes the dissipation, and S denotes user-defined terms for the turbulent kinetic energy (k) in equation 2.4 and for the specific dissipation rate (ω) of the turbulent energy in equation 2.5. These constants are identified by the corresponding subscripts of k and ω in respective equations. D_ω denotes the cross-diffusion term that facilitates the transition between two turbulence models k-ω and k-ϵ.

The standard k-ω, introduced by Wilcox et al. [41] uses linear equations to solve for the eddy viscosity, but has the disadvantage of high freestream sensitivity of the specific dissipation. In this respect, the Shear-Stress Transport (SST) variation of the k-ω has additional features that make it more robust in fluctuating flows [44, 45]. First, this model uses a standard k-ω approach for the near-wall boundary layer approximation using specific rate of dissipation (ω) of turbulence (essentially, the ratio of k to ϵ) in estimating the turbulence scale, which is one of the best formulations currently available. Second, it transforms into a k-ϵ formulation in the wake region of the boundary layer and free shear flow region to overcome the high sensitivity of dissipation. This is achieved through a blending function which acts as a gradual switch between k-ω and k-ϵ for the respective flow regions. Finally,

it modifies the formulation for turbulent viscosity (μ_t) to account for the principal turbulent shear stresses being transported in the wake region of the boundary layer. These features make the SST$-$ k-ω a more reliable and accurate two-dimensional model for approximating turbulence in engineering problems that are relatively simple but involves winder range of flow conditions such as adverse pressure gradient and transonic shock wave.

2.3 Adaptive mesh generation

A well-designed computational grid space is the foundation for a time-optimized simulation. Along with being able to approximate a flow solution accurately, an efficient numerical model should also try to reduce the time of computation. In a steady-state approach, this could be directly related to two aspects of the simulation - the number of numerical iterations, and the time taken for each iteration. In this respect, the concept of adapting the mesh during the simulation based on instantaneous solutions is important and is referred to as Adaptive Mesh Generation. This approach allows to refine or coarsen the mesh at any iterative step based on an evaluation of the flow properties at the instant. This promotes better accuracy through selective refinement and reduces time of computation by getting rid of redundant nodes.

It is essential to note that the meshes used in this study contain triangular elements arranged in an unstructured fashion (see figure 2.1). This is beneficial for the numerical process in two ways - ease of mesh generation with lesser time needed to generate the mesh as compared to structured meshes, and provides the additional option of solution-based adaptive mesh generation. ANSYS Fluent supports the use of unstructured meshes

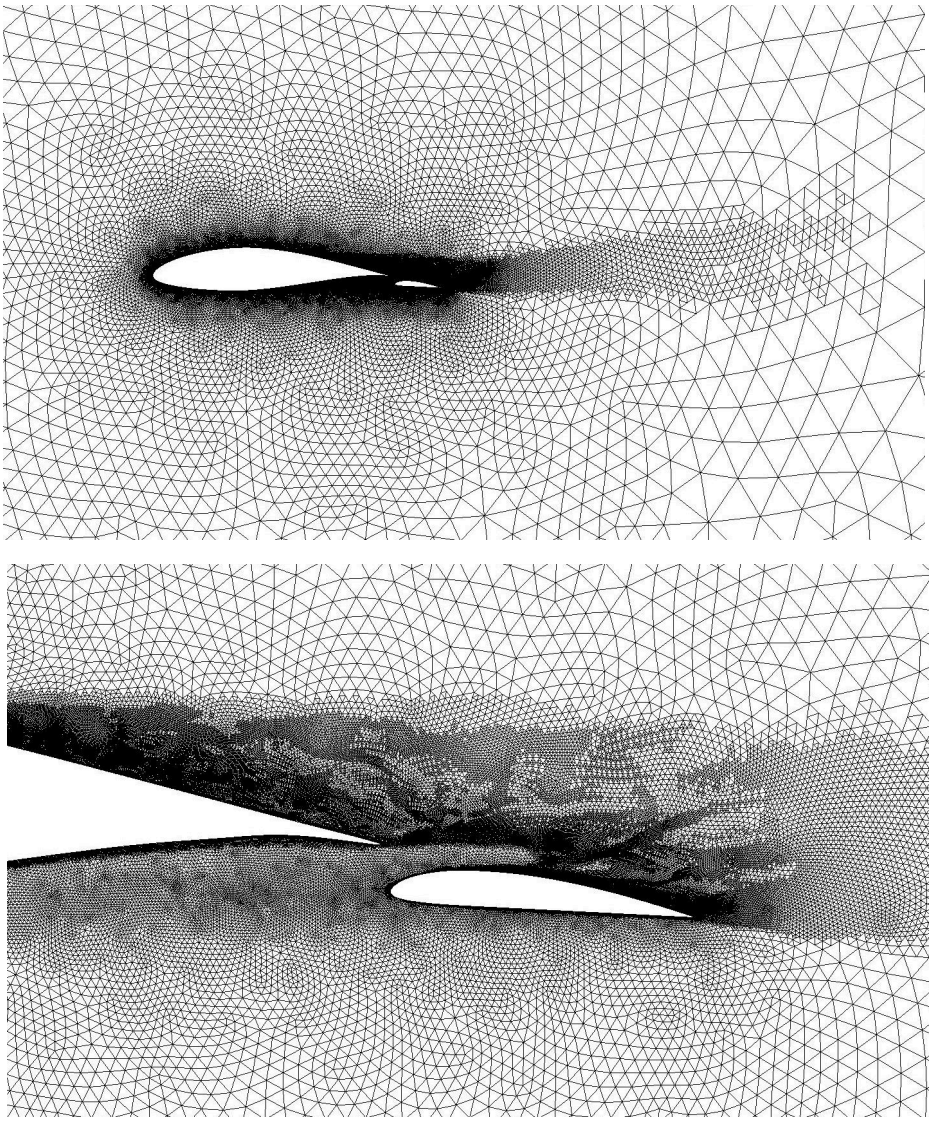

Figure 2.2: Illustration of mesh generated after dynamic grid adaption during simulation of NACA 64_3-618 airfoil with Clark Y trailing-edge flap actuated at $+5^\circ$, based on 'gradient'of velocity magnitude. Top panel: view of overall mesh refinement near the trailing-edge, bottom panel: a closer view of the mesh refinement near the airfoil-flap assembly.

for analysis and provides a few different ways of adaptive mesh generation, and is crucial for the two-dimensional study of multi-element airfoil. A comprehensive understanding of the aerodynamic behavior requires the assessment of a wide range of angles of attack and

variation in angles of actuation of the flow-control device, which provides a large pool of cases and reiterates the need for optimized computation of each case. The solution-based adaption in ANSYS Fluent allows both the addition of mesh elements (or cells) for resolving flow features more accurately, and removal of cells to promote faster convergence. By using a solution-based adaption, the refinement of the mesh is more optimized for the specific problem and hence prevents disproportionate grid densification and reduces the computation time for each iteration. In the bigger picture of the numerical computations, this allows an optimized used of computational resources and time.

The solution-based adaption is a two-staged process, where first the cells to be refined or coarsened are identified based on specific flow properties and then a selective adaption is implemented to generate the new mesh. The identification of the cells is done through an adaption function based on the values of certain flow quantities such as the gradient of velocity magnitude, the curvature of pressure gradient, and variation in wall shear stress. Some of the approaches used in ANSYS Fluent cover adaption based on the boundary conditions, gradient of flow quantities, and the iso-values in measured regions. When executed manually, adaption allows the user to view the mesh regions that will be modified before the adaption is initiated and this approach is called static grid adaption. One of the most important benefits of this two step process is the flexibility to experiment various adaption function without actually altering the original grid. ANSYS Fluent also allows the user to pre-define the adaption criteria in which case the adaption process becomes completely an automatic process in the course of the iterative process. The preset conditions would identify the flow property to be evaluated and iterative intervals for the evaluation that renders the adaption as a dynamic process and hence known as dynamic grid adaption. In the aerodynamic analysis of two-dimensional airfoils, flow velocity was identified as the most

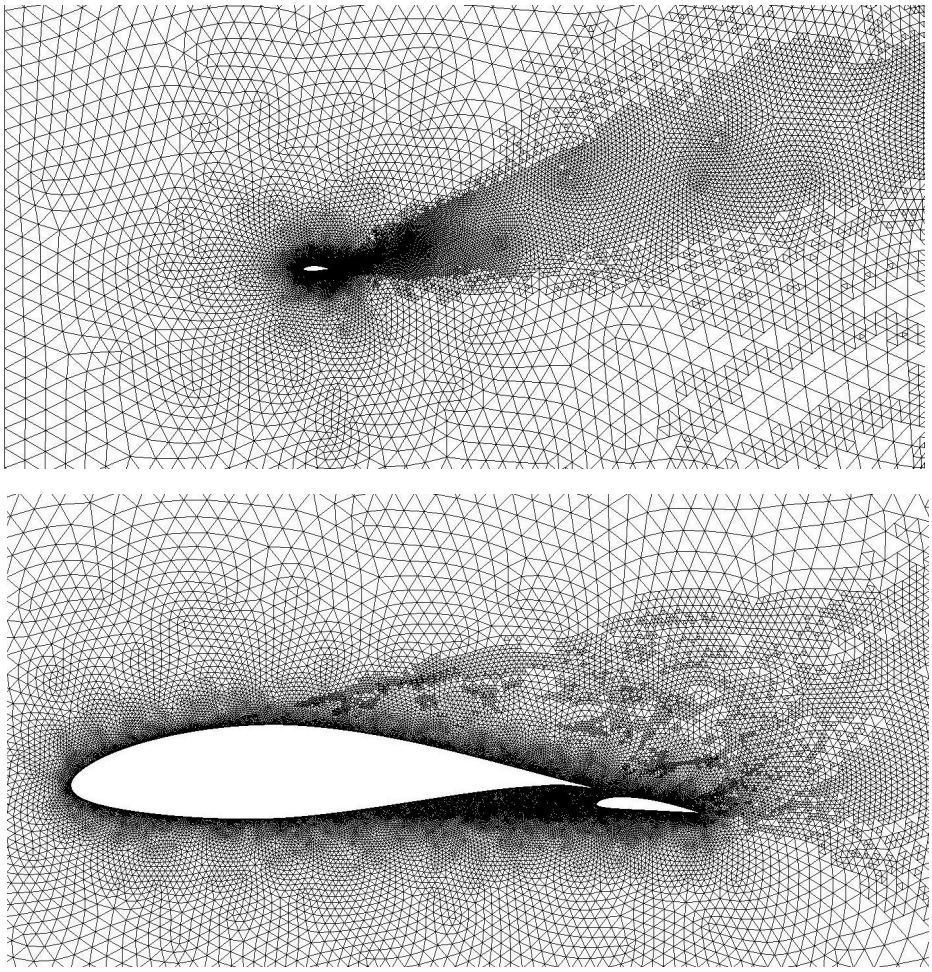

Figure 2.3: Illustration of mesh generated after dynamic grid adaption during simulation of NACA 64_3-618 airfoil with Clark Y trailing-edge flap actuated at $+5^\circ$, based on 'curvature'of velocity magnitude. Top panel: view of overall mesh refinement in the wake boundary, bottom panel: a closer view of the grid region surrounding the airfoil.

important property and measuring its gradient between adjacent cells as the methodology for solution-based grid adaption. And ANSYS Fluent also offers two distinct methods of gradient grid adaption, one based on the gradient of the property that measures the instantaneous slope of the curve, and the other using curvature, which essentially is the second derivative in the same frame of reference. Figure 2.2 shows an example of grid adaption

executed based on the gradient of velocity magnitude, and figure 2.3 show an example of curvature based adaption. Comparing the top panels of both figure, notice how the difference in the adaption function used causes different regions of the grid to be refined.

A brief guideline to make efficient use of this feature in ANSYS Fluent is provided here for the reader.

- ◇ The primary mesh must be sufficiently refined to represent important features of the geometry (for example, the airfoil profile as in this study).
- ◇ The initial mesh should be designed with attention to details such as average element size, node distribution on boundary conditions, etc. to allow ANSYS Fluent to adequately represent the average flow behavior accurately.
- ◇ The boundary conditions should be defined appropriately to represent the the physics of the flow correctly.
- ◇ The monitors observed during the iterative process should be selected correctly to assess the convergence of the solution appropriately.
- ◇ Being a solution-based approach, a convincing convergence should be attained for the initial solution before initiating grid adaption process.
- ◇ The flow property selected as a basis for the adaption should be carefully chosen, based on a good understanding of which features are important in the flow and what properties are good indicators of flow alterations. For example, the gradient of mean velocity might be able to represent an incompressible flow, whereas in case of a shock wave, it might be better to use the pressure gradients.

- ◇ Refinement of mesh should be carried out carefully, as overly dense meshes could result in poor accuracy due to generation of gradients higher than expected.
- ◇ In most cases, it is advisable to conduct a mesh independence study for the initial neutral mesh.
- ◇ Normalization of mesh adaption often makes the dynamic adaption process easier to setup. The gradient or curvature is bound by zero and upper limit of the selected property when the method of normalization selected is *normalize*.
- ◇ The interval between iterations selected for dynamic grid adaption should be chosen wisely to provide enough time (iterations) for each intermediate mesh to converge satisfactorily.
- ◇ The threshold values for refining and coarsening should be selected based on an understanding of the extend of flow alterations.

2.4 Computational approach

The process followed in a CFD analysis can be divided into 3 major steps - pre-processing, simulation, and post-processing. Pre-processing spans a wide range of task from designing the geometry to designing the computational grid, and setting up the solver for simulation. Most of the pre-processing is done using ANSYS Workbench, which is a project management tool with access to various applications for setting up the geometry and designing the mesh. The airfoil coordinates of each section to be analyzed are imported into the computer-aided design software DesignModeler to create a geometry of normalized chord length. The far-field boundaries are defined around the airfoil, with attention to inflow and

outflow regions replicating the external flow region. An optimized computational grid is generated for each geometry taking into consideration all the important aspects of mesh designing, including a careful mesh independence study as discussed in section 2.1. The computational grid is built using AnsysMeshing which provides various features to generate a numerically efficient meshes compatible across various platforms, including ANSYS Fluent.

Independent meshes are designed for each airfoil geometry to be analyzed by following a consistent mesh generation methodology to enable its use for the range of angles of attack being studied. Each mesh is imported into ANSYS Fluent and checked for the quality of the discrete elements and their assembly into the computational grid. The solver is setup for a two-dimensional steady-state pressure-based analysis in a planar spatial frame with absolute velocity formulations. The fluid for simulation as air with a standard density and a modified dynamic viscosity that is altered to match the Reynold's Number (Re) of the flow defined in the corresponding experimental reference studies. The boundary conditions are designed specifically for each case of the angle of attack studied, by defining the X (x_i) and Y (x_j) components of the relative velocity of wind incident on the airfoil section. For the two-dimensional analysis of airfoil sections, it was determined that the most appropriate model for turbulence would be the SST$-$ k-ω and is selected as part of setting up the solver for simulation.

In CFD simulations, it is critical to design a computationally feasible mesh that is also capable of capturing the properties of complex flows. Physical understanding of the flow around an airfoil is critical in this respect. Interaction of the flow with the airfoil tends to create disturbances in the flow, which are more prominent in the near-airfoil region than the far-field region. This understanding played a major role in the designing of initial meshes

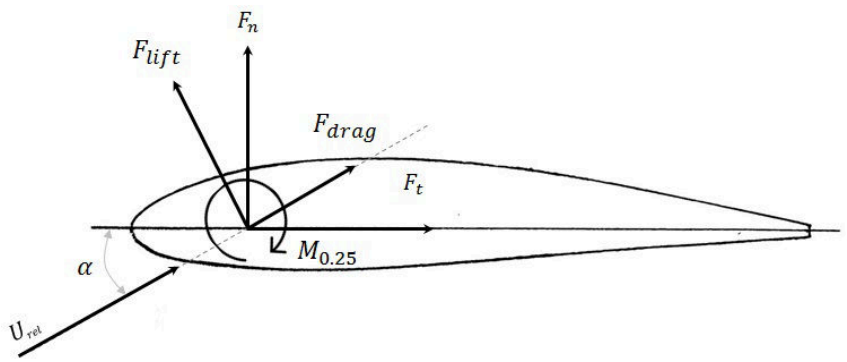

Figure 2.4: Wind turbine blade are subjected to certain forces and moments during operation, due to a pressure difference arising due to the airflow. The forces and moments reduced to a 2-dimensional airfoil sections are shown here.

for each airfoil geometry. At higher angles of attack, flow separation induces vortices that could significantly change the flow structures and properties in the airfoil wake. The initial mesh was designed with more nodes on the airfoil surface (smaller elements closer to the airfoil) and lesser nodes on the far-field boundaries (much bigger elements). Figure 2.1 shows an outward growth in mesh element size from the airfoil surface towards the far-field boundaries. The need for higher mesh density near to the airfoil surface and the trailing-edge inspired the adoption of selective mesh densification in ANSYS Fluent, as described in section 2.3. The idea was to reduce computational time for the entire domain of study by reusing a base mesh (initial mesh) for each case studied, and improving the mesh design (through dynamic adaption) for only the relevant angles of attack as the solution evolves. Treating each angle of attack studied as disparate cases, this helped reduced usage of resources for less complex flow scenarios, and optimized the computational time for more complex flow scenarios, by allowing the dynamics of the flow to decide the mesh regions that need (or does not need) refinement.

Numerical simulations are carried out in the grid space designed for flow around the airfoil sections. Convergence criteria for the numerical model is based on residuals for X velocity,

Y velocity, turbulent kinetic energy (k), and specific dissipation rate (ω). The most important aerodynamic properties of any airfoil section are the coefficients of lift and drag, which are continuously monitored through the iterative process to establish stability. As the simulation progresses through numerical iterations, dynamic mesh adaption is initiated if there is continued increase is the normalized residual values. This dynamic decision of adaption initiation could vary from the iterative perspective, depending on the angle of attack, flow scenario, and the angle of actuation of the flap. The mesh is then dynamically refined at regular intervals of iteration based on a normalized refinement criteria set on the velocity magnitude. Grid adaption with the method as gradient of velocity magnitude seems like a better model to capture the features of thickening of the boundary layer (figure 2.2 shows an example of the type of mesh for a NACA 64_3-618 airfoil with a Clark Y trailing-edge flap refined by this method). On the other hand, adaption by curvature of velocity magnitude seems superior to capture the flow structure and vortical features on the separated wake as we enter into stall (figure 2.3 depicts an example of the type of mesh for the same airfoil-flap assembly above, obtained by this method of refinement). A more critical situation could be the intermediate stage of separation and reattachment at specific angles of attack and actuation angles of the flap. A combined methodology of both gradient and curvature of velocity magnitude is necessary for mesh adaption in trying to capture the flow behavior in this flow regime transitioning from the attached flow to the separated flow. This incipient separation flow behavior consists of really thick boundary layer near the trailing edge as well as vortical structures in the wake of the airfoil.

Once the solution converges, post-processing options available in the solver are used to establish the consistency of the results with a physical understanding of the flow around the airfoil. This is carried out by studying the contour and vector plots of the significant

flow properties such as the velocity field, vorticity generation, and pressure gradient. Once a convincing convergence is obtained, the Lilienthal forces acting on the airfoil section are reported, which in turn are used to determine the coefficients of lift, drag. The pitching moment coefficients are computed from the moments around the Z-direction, reported at the quarter-chord length along the X-direction. As the key indicators of the aerodynamic behavior of each airfoil section, the coefficients of forces and moments are obtained based on the properties of the air flow incident on the airfoil using the below equations,

$$C_l = \frac{F_{lift}}{\frac{1}{2}\,\rho\,v^2\,c} \tag{2.6}$$

$$C_d = \frac{F_{drag}}{\frac{1}{2}\,\rho\,v^2\,c} \tag{2.7}$$

$$C_m = \frac{M_{aer}}{\frac{1}{2}\,\rho\,v^2\,c^2} \tag{2.8}$$

where C_l is the coefficient of lift, C_d is the coefficient of drag, C_m is the coefficient of pitching moment, c is the chord length of the airfoil section, ρ is the density of air, and v is the velocity magnitude of the relative wind noted as U_{rel} is the figure 2.4. Also, M_{aer} indicates the pitching moment acting on the airfoil due to the aerodynamic forces acting at the aerodynamic center, which is indicated as $M_{0.25}$ in the figure 2.4. F_{lift}, F_{drag} are the aerodynamic forces of lift and drag respectively acting on the airfoil section as a result of the pressure difference arising from the flow around it, and are computed from the Lilienthal forces reported in the solver as:

$$F_{lift} = -F_t \sin(\alpha) + F_n \cos(\alpha) \tag{2.9}$$

$$F_{drag} = F_t \cos(\alpha) + F_n \sin(\alpha) \tag{2.10}$$

where α is the angle of relative wind in degrees ($^\circ$), F_t, F_n are the Lilienthal forces acting on the airfoil section in the tangential and normal directions.

Chapter 3

Validation Study

The numerical procedure to compute aerodynamic characteristics of airfoils equipped with trailing-edge flaps was established from a validation study. NACA 23012 airfoil attached with a Clark Y flap is a classical well-studied example of a multi-element airfoil-flap assembly used in aeronautical applications. The computational grid setup using ANSYS Workbench defines the flow field around the airfoil geometry. The leading edge of the airfoil corresponds to the origin of the geometry and the far-field is defined by a rectangle defined around it. Flow inlet is defined on the face (edge) ahead of the airfoil as the front edge and on two edges above and below the airfoil section geometry. The front, top, and bottom edges independently measure a distances of 10 times the chord length from the origin where the leading-edge of the airfoil is located. The fourth edge of the rectangle defines the exit of the airflow as a pressure outlet and is located at a distance 20 times the chord length, measured from the trailing edge. Taking care to optimize the computational time for the simulation, an unstructured triangular mesh is generated as the computational grid space through the AnsysMeshing application.

Global mesh settings in AnsysMeshing has features targeting appropriate capture of flow interactions for specific flow solvers such as the ANSYS Fluent. Local mesh settings are used to set the right combination of node assembly on the grid space to enable denser mesh closer to the airfoil where the fluid-structure interaction is most important. The size for far-field region, and the global and local mesh settings were determined through mesh independence studies conducted independently for airfoils - NACA 23012, NACA 64_3-618, and DU 93-W-210 in their original configurations. A similar approach consistent with the knowledge obtained from meshing original airfoil configurations was used in the development of meshes for multi-element configurations with a 20% chord Clark Y shaped flap section. One of the initial meshes designed in this manner was shown in figure 2.1 in chapter 2 as an example of a mesh used to initiate the numerical simulation before dynamic adaption is initiated.

Two distinct configurations for the airfoil section equipped with a flow-control device were analyzed as part of standardizing the numerical procedure. The numerical results are interpreted through a study of graphical plots of aerodynamic coefficients, comparing them with experimental data for a particular range of angles of attack. The coefficients of lift and drag were matched to establish the systematic procedure for assessing airfoil sections with and without flaps. The calculations were made for normalized airfoil sections in a normalized air velocity field using standard density of air and a modified dynamic viscosity in order to match the Reynold's number. The model adopted is a standardized numerical analysis of a non-dimensionalized airfoil section placed in a normalized flow field of air with standard density and the dynamic viscosity (μ) altered to match the Reynold's number and the turbulence intensity ratio retrieved from the experimental data used as reference for this study.

3.1 NACA 23012 Validation case

ANSYS Fluent was used for flow simulation of NACA 23012 airfoil section in two distinct configurations with an attached trailing-edge fractional chord flap of Clark Y profile - actuated at -5° and $+20^{\circ}$. Actuation angle here, refers to the relative angle between the chord lines of the main airfoil section and the trailing-edge flap section, measured from the airfoil chord line. An extensive study of various configurations (reported by Platt [2]) was used as the basis for the optimum location for a Clark Y flap near the trailing edge of NACA 23012. This particular configuration of airfoil-flap assembly used in the numerical study is shown in figure 3.1. This configuration was the result of a detailed experimental assessment of various configurations to determine the optimum gap between the airfoil and the flap. The relative position of the flap is extremely important in modifying the airfoil behavior in two aspects - alteration in the camber of the effective airfoil profile, and flow properties near the trailing edge. The presence of a trailing-edge flap forms a new effective airfoil profile with a modified camber, which plays an important role in quantifying the pressure difference on the upper and lower surfaces, which in turn dictates the aerodynamic coefficients. The gap between airfoil trailing-edge and flap nose characterizes an accelerated jet capable of revitalizing the boundary layer by re-attachment of separated flow on to the flap section. These flow modification have direct impact on the aerodynamic characteristics of the airfoil-flap assembly.

Results from the numerical study of NACA 23012 with Clark Y trailing-edge flap are reported in figure 3.2 when the flap is actuated at -5° and figure 3.3 when flap is actuated at $+20^{\circ}$. The results shown here indicate that the numerical computations are comparable to

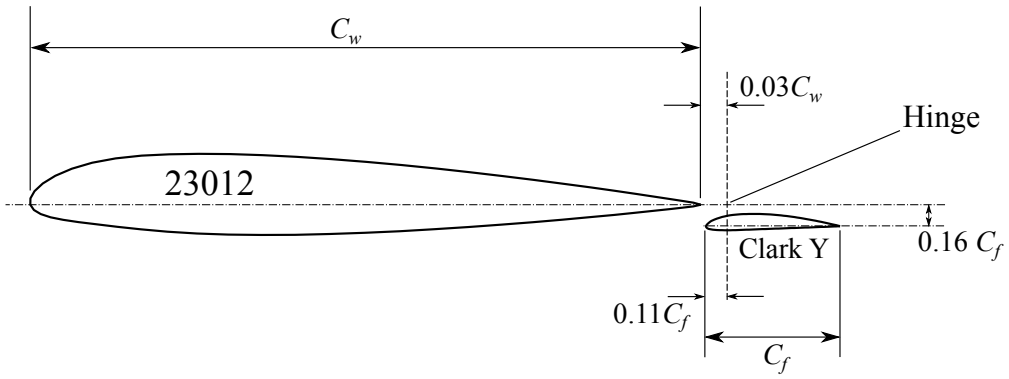

Figure 3.1: Assembly of airfoil and trailing-edge flap for NACA 23012 with Clark Y flap (adapted from [2])

the aerodynamic characteristics reported through experimental studies conducted by NACA and published by Platt [2]. Both the configurations of airfoil-flap assembly were studied for angles of attack in the range of -6° to $+26^\circ$, reporting the aerodynamic coefficient at every 2°. This spans a major regime of flow that an airfoil in the aerodynamically active parts of a wind turbine blade would be subjected to. Notice the drop in lift characteristics beyond $\alpha = +15^\circ$ in both figures 3.2 and 3.3, which indicate a regime of flow with separated boundary layer. The high angles of attack causing boundary layer separation is the primary cause for a drop in lift generation along with other effect such as increased form drag and vortex shedding. A closer observation of the top panels of these figures indicate reliable approximation of lift coefficients throughout the regime of study, even in the regions of the plot that indicate separated flow. The numerical approximation of drag behavior of airfoil sections are a delicate aspect in itself, especially in the case of highly separated flows. In this respect, it should be noted from the bottom panels of figures 3.2 and 3.3 that the model is capable of estimating the drag coefficients with reasonable accuracy, barring acceptable limits of numerical approximation errors.

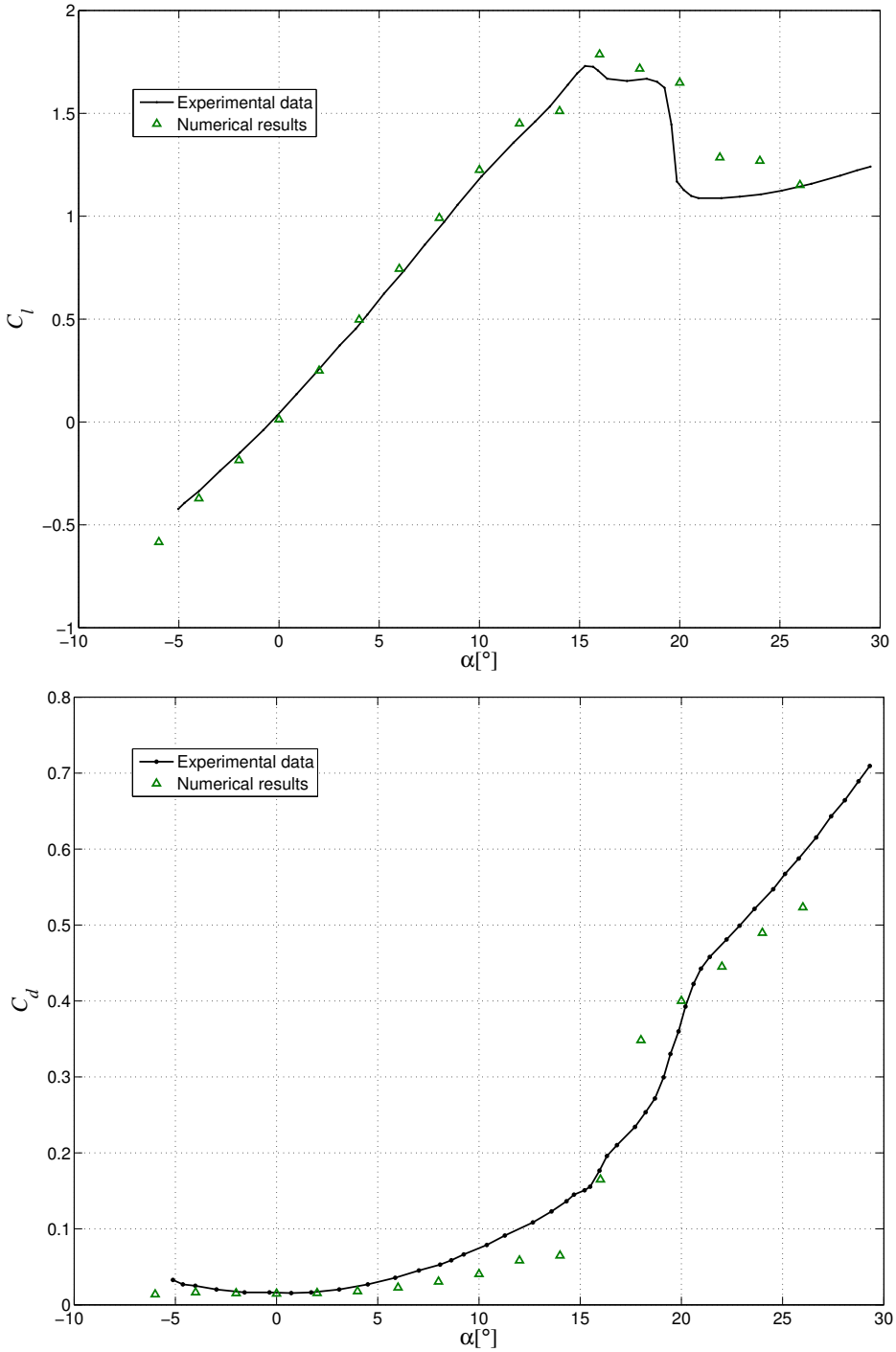

Figure 3.2: Numerical results for aerodynamic coefficients of a NACA 23012 airfoil section with trailing-edge flap Clark Y actuated at -5°, compared with experimental results [2]. Top panel: lift coefficient C_l, bottom panel: drag coefficient C_d, both plotted against angle of attack α.

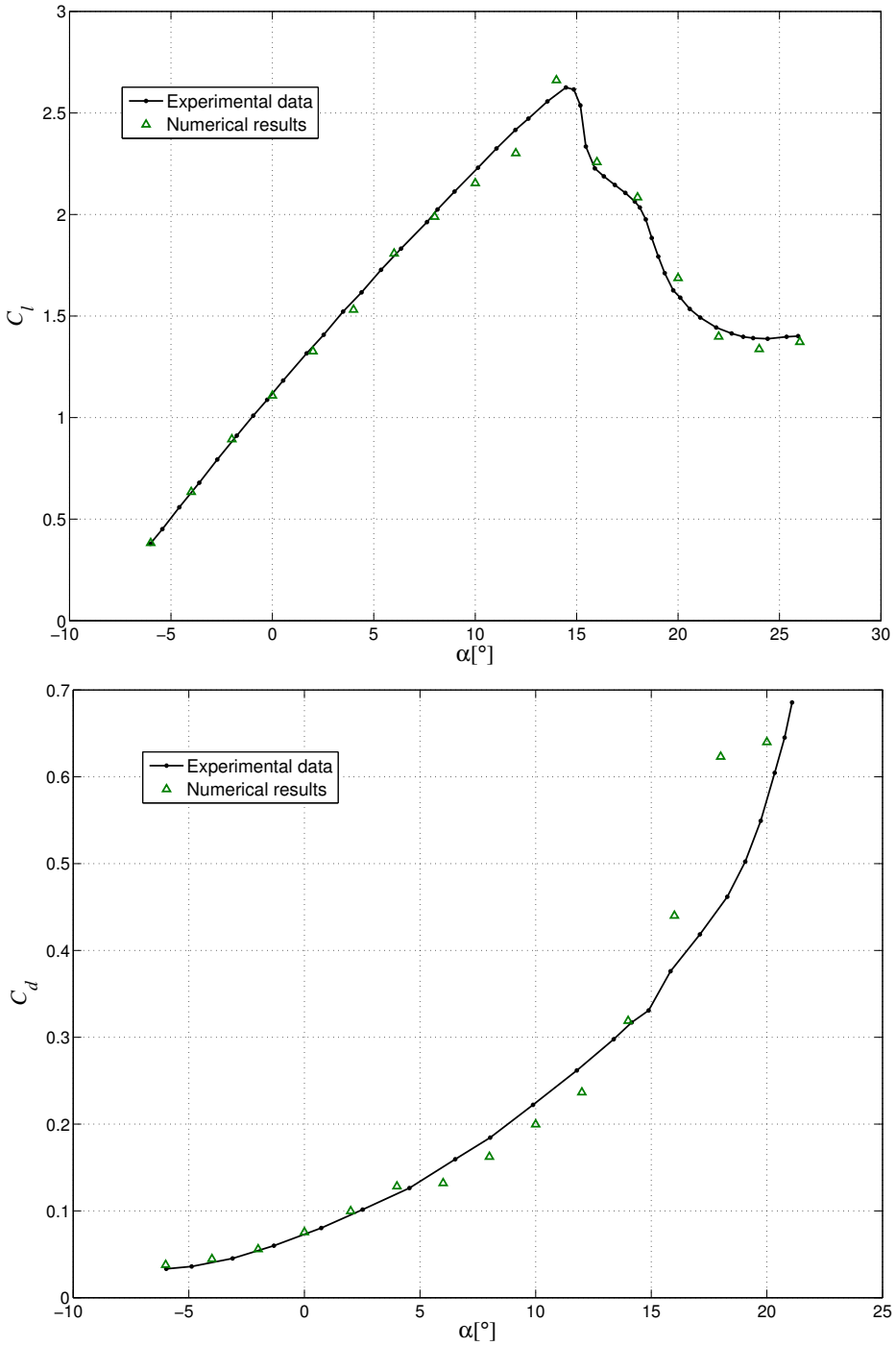

Figure 3.3: Numerical results for aerodynamic coefficients of a NACA 23012 airfoil section with trailing-edge flap Clark Y actuated at $+20°$, compared with experimental results [2]. Top panel: lift coefficient C_l, bottom panel: drag coefficient C_d, both plotted against angle of attack α.

These characteristic plots establish the ability of the numerical approach to make significantly reliable computational approximations of aerodynamic characteristics of airfoils with trailing-edge flaps. An important observation for the airfoil-flap assembly configurations is the variation in lift characteristics at different angles of actuation, especially the differences when the flap is actuated in negative and positive directions. This is relevant to the current study as implementation of trailing-edge flaps in wind turbine application is not intended to merely generate more lift, but also to optimize blade operation for power generation, which essentially indicates situations where the lift generation should be limited to avoid over-powering of turbine rotors. Agreement with experimental results shown here establishes the robustness of the numerical model and forms the platform to study modified airfoil sections designed to be used in futuristic wind turbine blades.

Chapter 4

Numerical Experiments

Flow-control devices such as the trailing-edge flaps are capable of changing the aerodynamic behavior of airfoil sections that are aerodynamically designed to generate significant lift. The extend of alteration however depends on the relative angle between airfoil and flap sections (actuation angle, β) and the angle of relative wind (angle of attack, α). This behavior of airfoil section was validated using aerodynamic simulations carried out using ANSYS Fluent for NACA 23012 in chapter 3. The kernel of this dissertation targets a similar study of two airfoil sections relevant to wind turbine blades. The traditional blades used on the NREL-5MW RWT was adopted as a baseline reference for such a study. The NREL-5MW RWT is a benchmark turbine for contemporary research on large utility-scale HAWT wind turbines. A schematic representation of the blade is shown in figure 4.1 pictorially indicate the length of the blade, relevant aerodynamic sections, and their respective span positions. Table 4.1 provides the list of airfoil sections used in these stations points, and indicate their distances from the root of the blade, and the respective chord lengths.

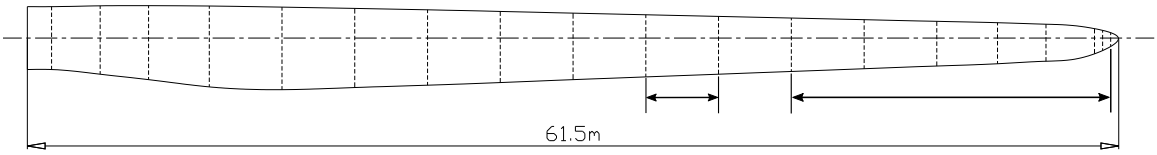

Figure 4.1: Aerodynamic stations on a standard blade used for NREL-5MW RWT with identifying also the prospective span regions to implement the flow-control devices.

The most inboard sections close to the blade root have cylindrical profile for uniform distribution of the loads where the blades are connected to the rotor hub. The aerodynamic station on the blade span that uses a designed airfoil profile is identified at station number 5, where a DU 00-W-401 airfoil is used. These airfoils are designed to interfere as less as possible with the aerodynamics of the rotor and with the primary purpose of reinforcing structural stability. The *Ellipsoid-1* and *Ellipsoid-2* are designed to provide a smooth transition to the outer blade profile from a cylinder to the DU 00-W-401 airfoil. The profiles of the six airfoil sections used on the standard blade for NREL-5MW RWT are shown in figure 4.2.

Two key airfoil sections used on the 61.5 m long blade in this machine are NACA 64_3-618 and DU 93-W-210 and their profiles are highlighted in figure 4.2. The NACA airfoil is used in a more aerodynamically active span section of the blade. The DU airfoil on the other hand, is a key airfoil section in the span region that transitions from an aerodynamically active part of the blade to the structurally stable part. The figure 4.1 provides a pictorial representation of the prospective sections along the span that could be modified with the flow-control device attachments. To identify the airfoil sections used in these noted parts of the blade, one entry of each relevant profile are highlighted in the table 4.1. The aerodynamic study covers a range of angles of attack relevant to the normal operating conditions of wind turbines. Information obtained from the study of these modified airfoil sections

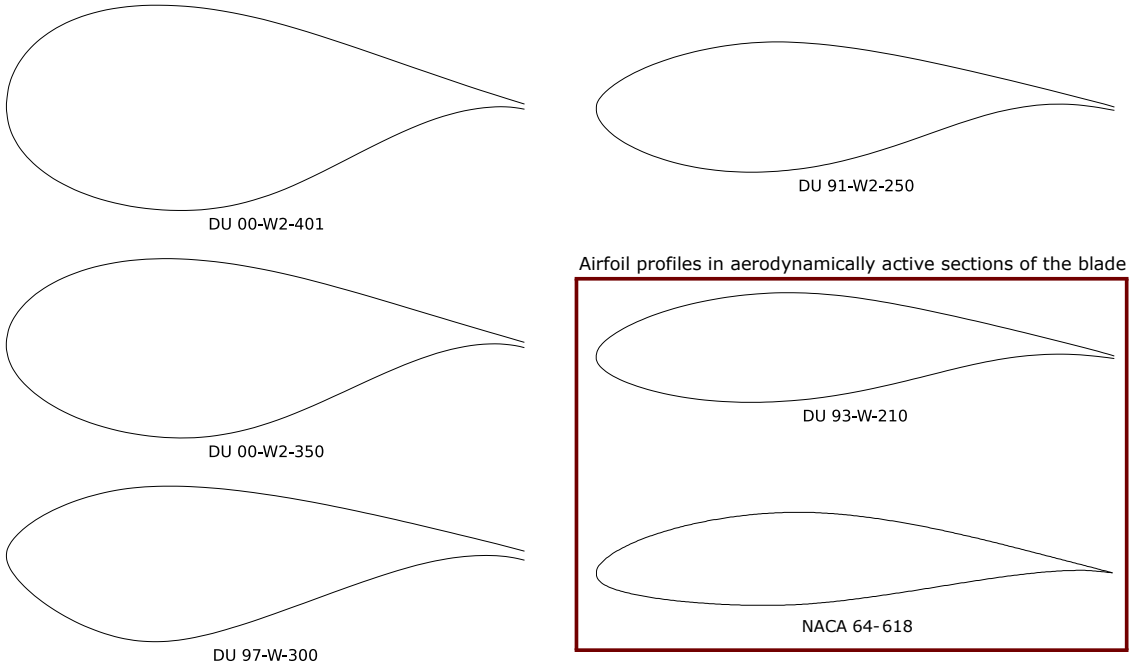

Figure 4.2: Profiles of the airfoil sections used to define the geometry of the NREL-5MW RWT blade. Left panel: top to bottom shows thick airfoils used in the inboard span regions from aerodynamic stations 5 to 8, right panel: top to bottom shows airfoils used in the mid-span to tip regions of the blade. Airfoils used in the most aerodynamically active sections are highlighted.

give a comprehensive understanding of lift, drag, and pitching moment behavior of airfoil sections equipped with an actuated trailing-edge flap. Understanding the effects of using a trailing-edge flap on these two airfoil sections provides valuable aerodynamic information relevant to the entire blade operation.

4.1 Study of NACA 64_3-618

Airfoil sections such as the NACA 64_3-618 are designed to be aerodynamically efficient, which essentially means in optimum operating conditions the lift-to-drag ratio is relatively

Table 4.1
Aerodynamic blade section distribution

Station	Span location [m]	Chord length [m]	Airfoil identifier
1	0	3.5420	Cylinder
2	1.3653	3.5420	Cylinder
3	4.1020	3.8540	Ellipsoid-1
4	6.8327	4.1670	Ellipsoid-2
5	10.2520	4.5570	DU 00-W-401
6	14.3480	4.6520	DU 00-W-350
7	18.4500	4.4580	DU 00-W-350
8	22.5521	4.2490	DU 97-W-300
9	26.6480	4.0070	DU 91-W-250
10	30.7500	3.7480	DU 91-W-250
11	34.8520	3.5020	**DU 93-W-210**
12	38.9479	3.2560	DU 93-W-210
13	43.0500	3.0100	**NACA 64-618**
14	47.1521	2.7640	NACA 64-618
15	51.2480	2.5180	NACA 64-618
16	54.6673	2.3130	NACA 64-618
17	57.3980	2.0860	NACA 64-618
18	60.1347	1.4190	NACA 64-618
19	60.5898	1.1395	NACA 64-618
20	61.0449	0.7787	NACA 64-618

higher. The airfoils NACA 64-618 and NACA 64_3-618 are essentially the same with minimal modifications that have negligible effects on the aerodynamics. As noted in the table 4.1 above, this forms the single largest airfoil section used on the standard blade for an NREL-5MW RWT, measuring the span length covered by it ($18\ m$). Due to the aerodynamic advantages brought out by this airfoil design, NACA 64_3-618 has gained prominence in turbine blade designs for various contemporary wind turbines [5, 40]. Such airfoil sections are the core of the *aerodynamically active* span sections of wind turbine blades and the primary contributors to the driving torque. However, these airfoils could be subjected to a wide range of aerodynamic loading conditions during the regular operation of a turbine blade and would not be able to operate in the optimum states for the entire range of

operation. The need to use flow-control devices arises here by which the modified airfoil sections could provide a wider range of operational conditions to work with.

Computational studies were conducted to evaluate the aerodynamic behavior of the NACA 64_3-618, when equipped with a trailing-edge flap. A 20% chord flap with Clark Y profile was selected to provide flexibility of active control. The relative location for the flap actuating hinge was obtained from similar studies conducted on a NACA 23012 airfoil section. To establish a standardized procedure, computation of aerodynamic characteristics were first carried out for the airfoil in its original configuration without any flow-control devices attached. The numerical results obtained from the simulation were validated through a direct comparison of the coefficients for each angle of attack reported. Figure 4.3 shows the results of such a comparison for the airfoil using experimental results reported by Abbott and Doenhoff [3] as a reference. Numerical simulations were completed in an environment setup with standard air density and modified dynamic viscosity for a flow field normalized by velocity to match a Reynold's number of 6×10^6. The computations were completed for a range of angles of attack from -6° to $+26^\circ$, which cover a significant range of operating conditions for the turbine blade sections where the modified sections would be used. The airfoils deployed on a wind turbine blade are subjected to relatively moderate angles of wind (unlike the need to generate very high lifting forces in aeronautic applications) and hence justifies the range of angle of attacks studied. The aerodynamic coefficients for the airfoil equipped with flow-control devices were computed for three configurations of the airfoil-flap assembly, with the trailing-edge flap actuated at -5°, 0°, and $+5^\circ$. Drawing a similar comparison to aeronautical applications on the use of flow-control devices, these trailing-edge flaps on wind turbine blades are intended to provide relatively

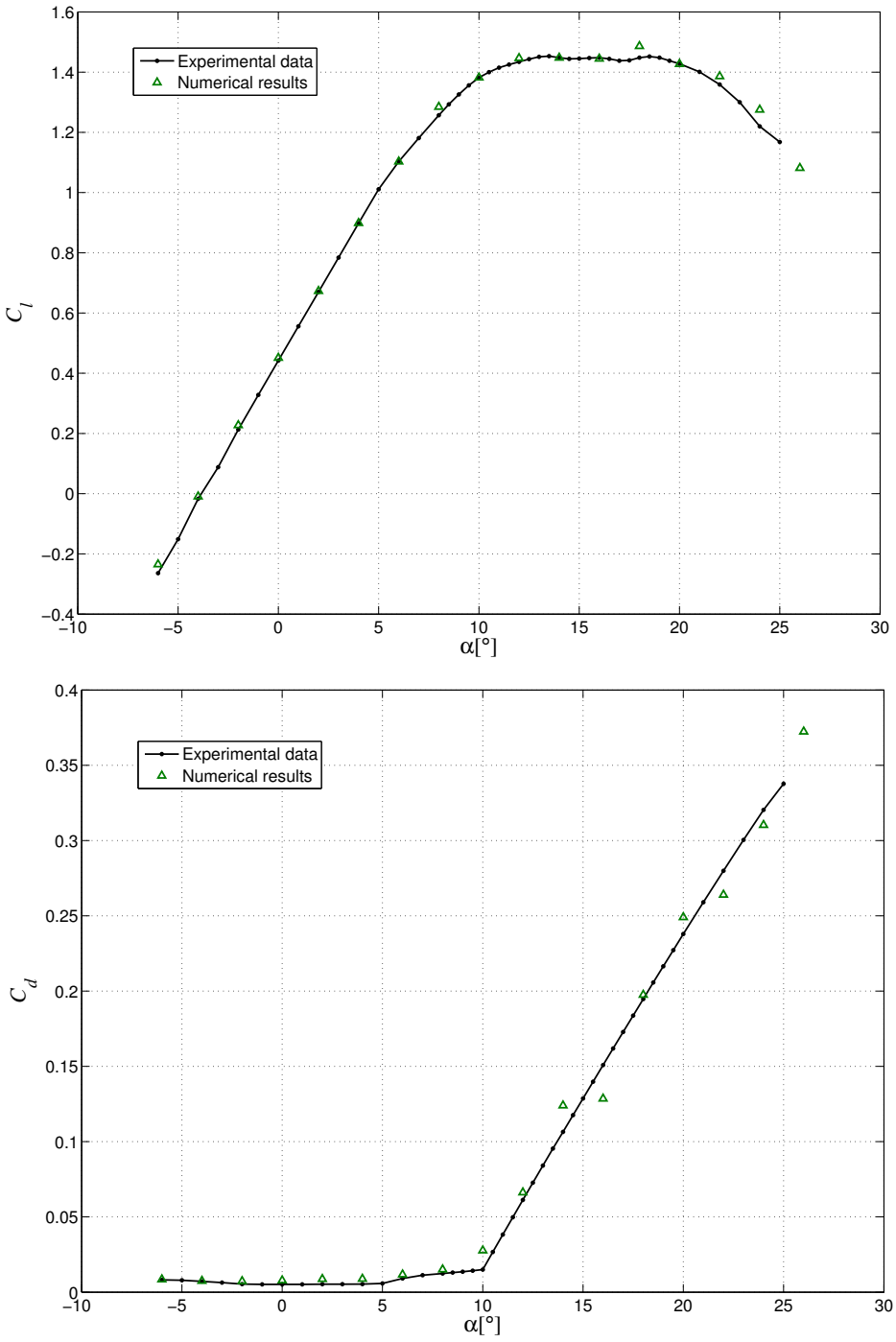

Figure 4.3: Numerical results for aerodynamic coefficients of the NACA 64_3-618 airfoil section compared with experimental results [3]. Top panel: lift coefficient C_l, bottom panel: drag coefficient C_d, both plotted against angle of attack α.

less increments of lift per unit length. The range of actuation angles covered in the current study is a modest approach to altering the behavior of the airfoil and can be extended to higher actuation angles (both in positive and negative directions). As noted before, the most important coefficients characterizing the aerodynamic behavior of airfoil sections are the coefficients of lift, drag, and momentum, which were reported in steps of 2° within the range of angles of attack studied. The discrete values of coefficients reported from the numerical study indicates comparability to the experimental results and hence, shows consistency in numerical approximation for the regime of flow studied. This also justifies the extension of the approach to compute aerodynamic characteristics of NACA 64_3-618 equipped with trailing-edge flaps.

In the evaluation of airfoil-flap assemblies, the numerical approach used for NACA 64_3-618 in its original configuration was extended with slight modifications to incorporate the use of trailing-edge flaps. The key indicators of aerodynamic characteristics are reported for the airfoil-flap assembly at three angles of actuation (β), covering the same range of angles of attack (α). The simulations were run in a numerical environment setup in the same manner to obtain a Reynold's number of 6×10^6. The primary contributors to modification in behavior, which are the coefficients of lift, and drag are reported in figure 4.4 for NACA 64_3-618 with the Clark Y profile trailing-edge flap actuated at three different angles, -5°, 0°, and $+5^{\circ}$. They are reported along side the experimental behavior plot (indicated as the 'No flap') for a qualitative assessment of the change in behavior brought about by the presence of the flap. Lift and drag forces, which are the most important component in determining the driving torque for the wind turbine operation are directly dependent on these coefficients. The significance of the alteration in the aerodynamic behavior is hence

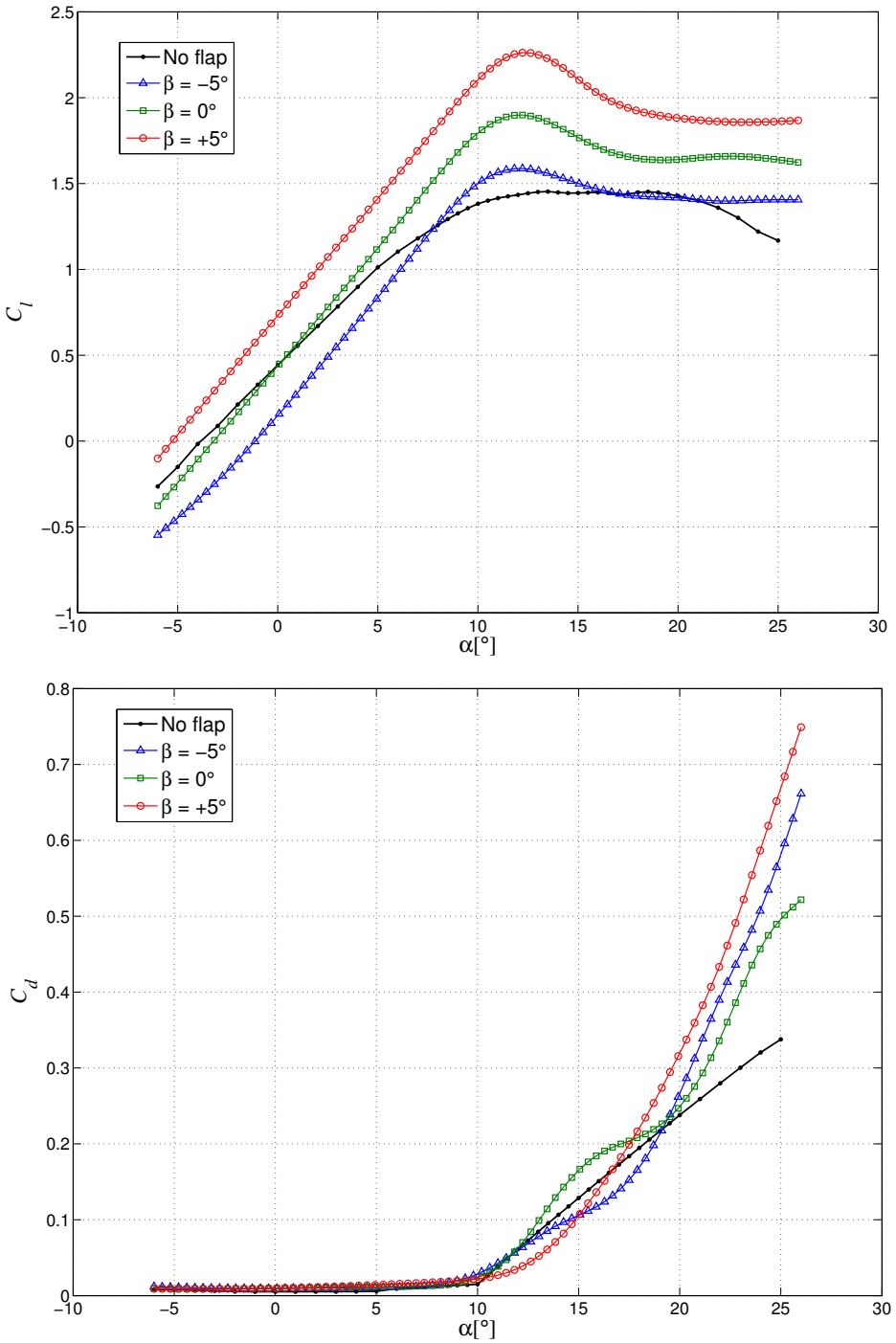

Figure 4.4: Numerical results for aerodynamic coefficients of a NACA 64_3-618 airfoil section with trailing-edge flap Clark Y actuated at $-5°$, $0°$, and $+5°$. Experimental data for the 'No flap' configuration are included for reference. Top panel: lift coefficient C_l, bottom panel: drag coefficient C_d, both plotted against angle of attack α.

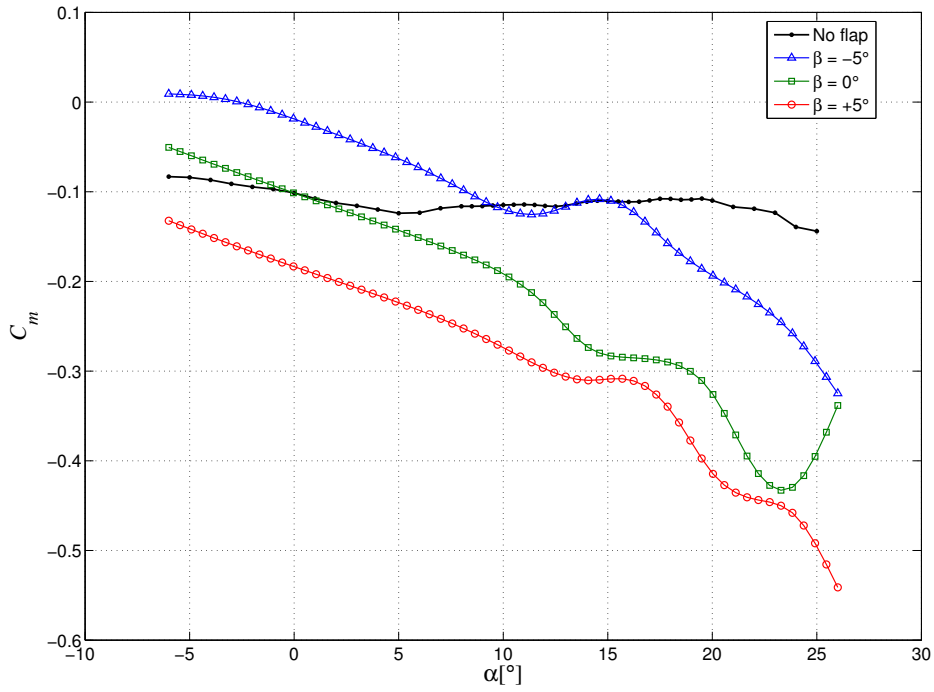

Figure 4.5: Numerical results for aerodynamic coefficients of pitching moment C_m, reported for NACA 64_3-618 airfoil section with trailing-edge flap Clark Y actuated at $-5°$, $0°$, and $+5°$, plotted against angle of attack α. Experimental data for the 'No flap' configuration is included for reference.

noticeable from the lift and drag plots. The corresponding coefficients of pitching moment for the same configurations are reported in figure 4.5. These moment coefficients are reported at quarter-chord length from the leading-edge of the main airfoil, which is a standard procedure in airfoil aerodynamics. That is, for a $1\ m$ long airfoil section it would be reported at $0.25\ m$ from the leading-edge.

Characteristics of the modified airfoil section with flap actuated at $-5°$ is has some relevance in the context of reducing aerodynamic and vibration loads that will act on the rotor during operation. Qualitatively, an overall reduction in lift coefficient can be observed for this configuration, in comparison with the original configuration. In the boundary-layer-attached regime of flow, which could be defined from $\alpha = -6°$ to $+10°$ (see figure 4.4),

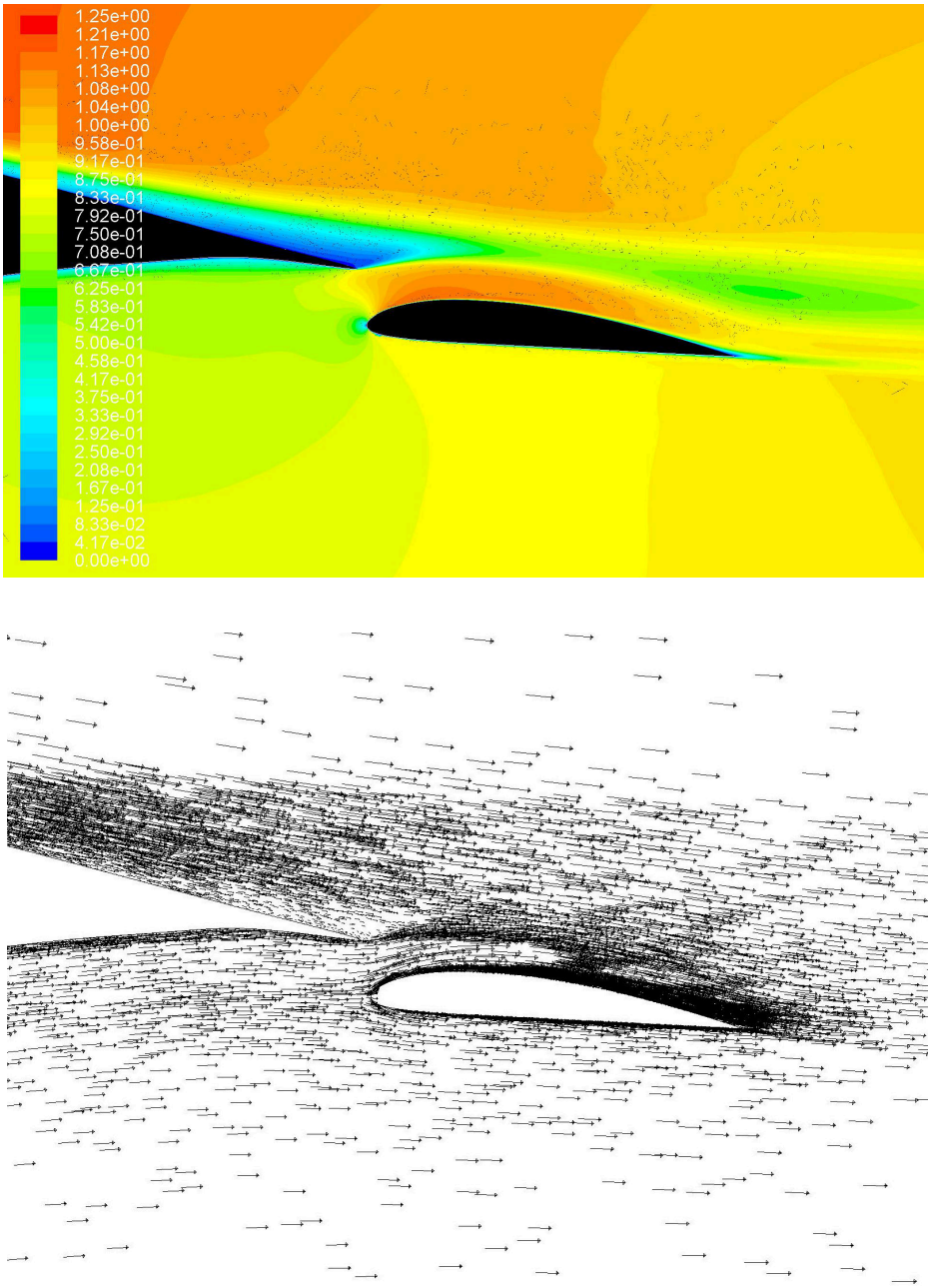

Figure 4.6: Qualitative representation of significant flow features near the trailing edge of flap actuated airfoil configuration of NACA 64_3-618 with Clark Y actuated $+5°$ at angle of attack $\alpha = +8°$. Top panel: Contour plot of velocity magnitude; Bottom panel: Vector plot of velocity magnitude.

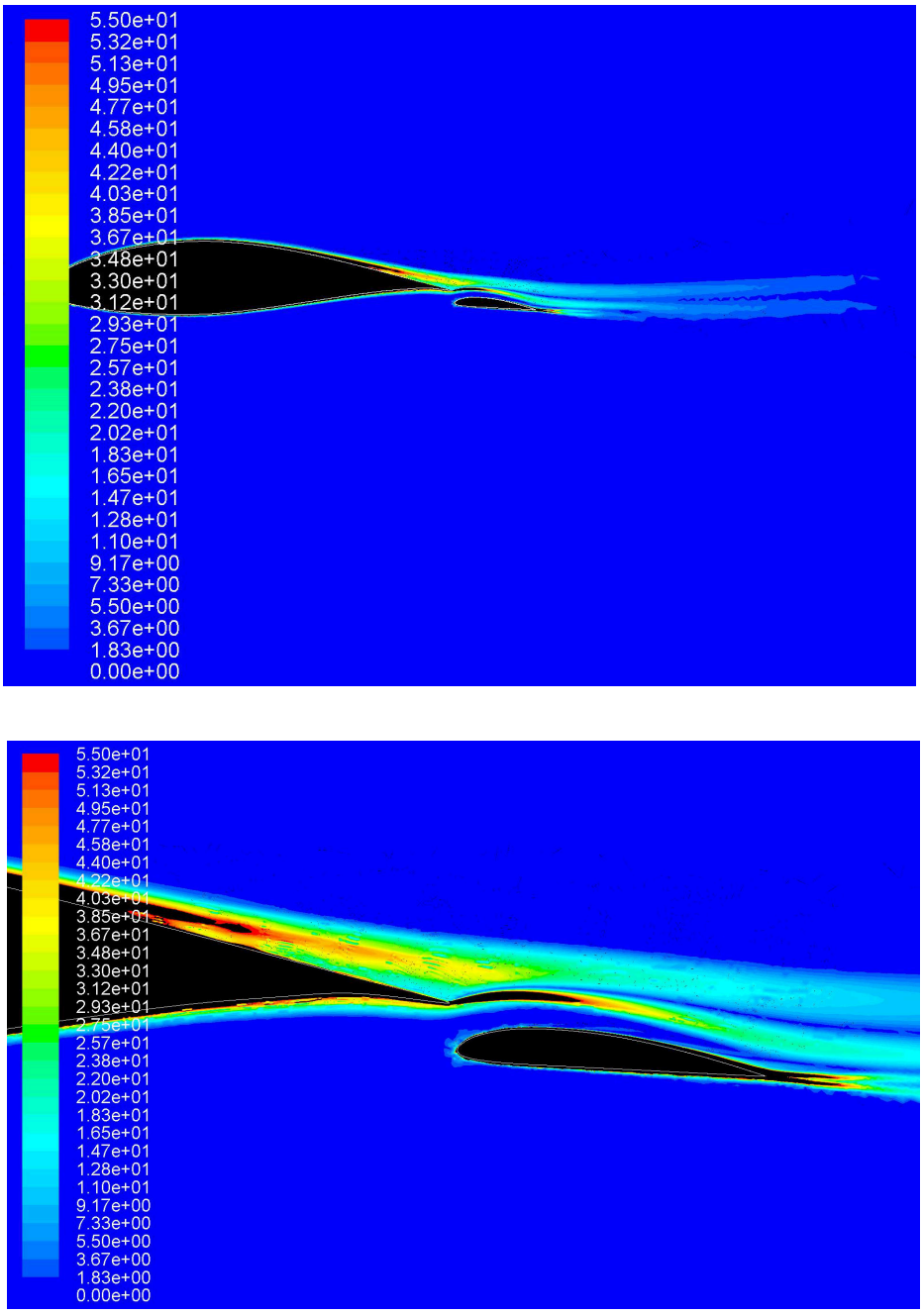

Figure 4.7: Qualitative representation of significant flow features near the trailing edge of flap actuated airfoil configuration of NACA 64_3-618 with Clark Y actuated $+5^\circ$ at angle of attack $\alpha = +8^\circ$. Top panel: Global view of contour plot of vorticity magnitude; Bottom panel: Closer view .

there is a noticeable drop in the lift. This can be explained by the increase in the gap between the airfoil and flap due to an actuation in the nose down orientation (i.e. $\beta = -5^{\circ}$). The results here indicate that the use of modified airfoil section in an operational turbine blade could benefit from this configuration, in dissipation of a lot of the lift generated due to increase in wind speeds. In contrast, the flap actuated at $+5^{\circ}$ contributes towards lift increments, which is a logical result of the high momentum flow arising from the narrow gap as a result of the nose-up orientation of the flap (i.e. $\beta = +5^{\circ}$). Figure 4.4 also indicates that 0° actuation of the flap can act as a neutral position for the modified airfoil section and maintains a lift behavior closer to the 'No flap' scenario. This configuration is consistent with effecting a delay in the onset of stall as in other configurations, and is important even for the neutral scenario. This delay is characteristic of slotted flaps and is a result of the revitalization of the flow near the trailing edge through reattachment of the boundary layer. The jet-like-flow near the trailing-edge helps in bringing about this phenomena, which is the result of the gap present between the airfoil and the flap (see figure 4.6 for visualization of flow structures). Actuating the flap from a neutral position of $\beta = 0^{\circ}$, to $+5^{\circ}$ or -5° presents a range of control-ability of the flap to either increase or decrease lift generation, respectively. The bottom panel of figure 4.4 indicates that this flexibility in lift generation are achieved with relatively insignificant increase in the drag characteristics in low angles of attack. At higher angles of wind ($\alpha > +14^{\circ}$) as the airfoil slips into stall, a drop in lift generation is observed. This is typical of airfoils and is the result of the drop in pressure difference, which is caused by various flow behaviors such as boundary layer separation, vortex shedding, and turbulent wake. However, with the flap attached near the trailing edge, the lift behavior attainable under stall conditions of operation has more flexibility. At higher angles of attack prior to stalling, the increase in lift coexists with higher drag

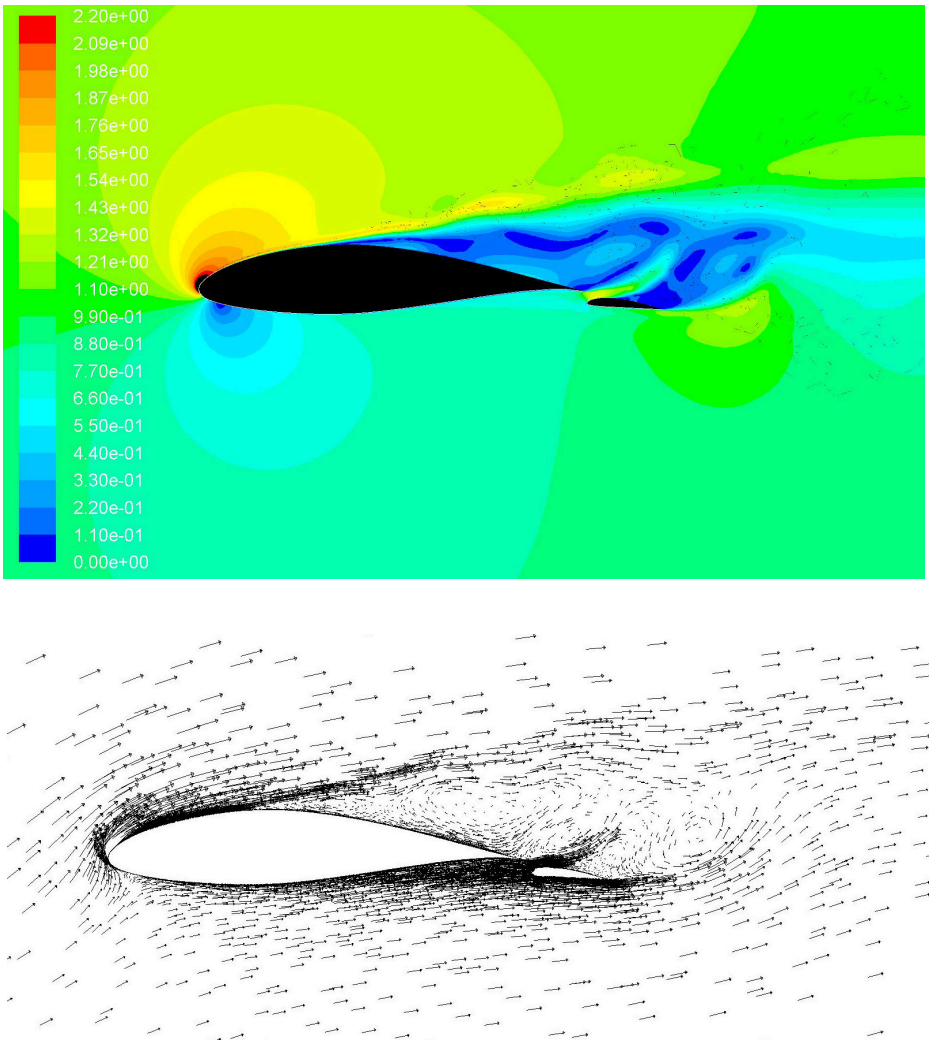

Figure 4.8: Qualitative representation of significant flow features around the flap actuated airfoil configuration of NACA 64_3-618 with Clark Y actuated $+5^\circ$ at angle of attack $\alpha = +16^\circ$. Top panel: Contour plot of velocity magnitude; Bottom panel: Vector plot of velocity magnitude.

coefficients that is typical in multi-element airfoil configurations. The NACA 64_3-618 airfoil section that is used in the most "aerodynamically active" parts of wind turbine blades could be subjected to both low angles of attack and stall conditions in standard operating conditions and hence, the use of a trailing-edge flap will provide more control-ability to these span sections of the blade.

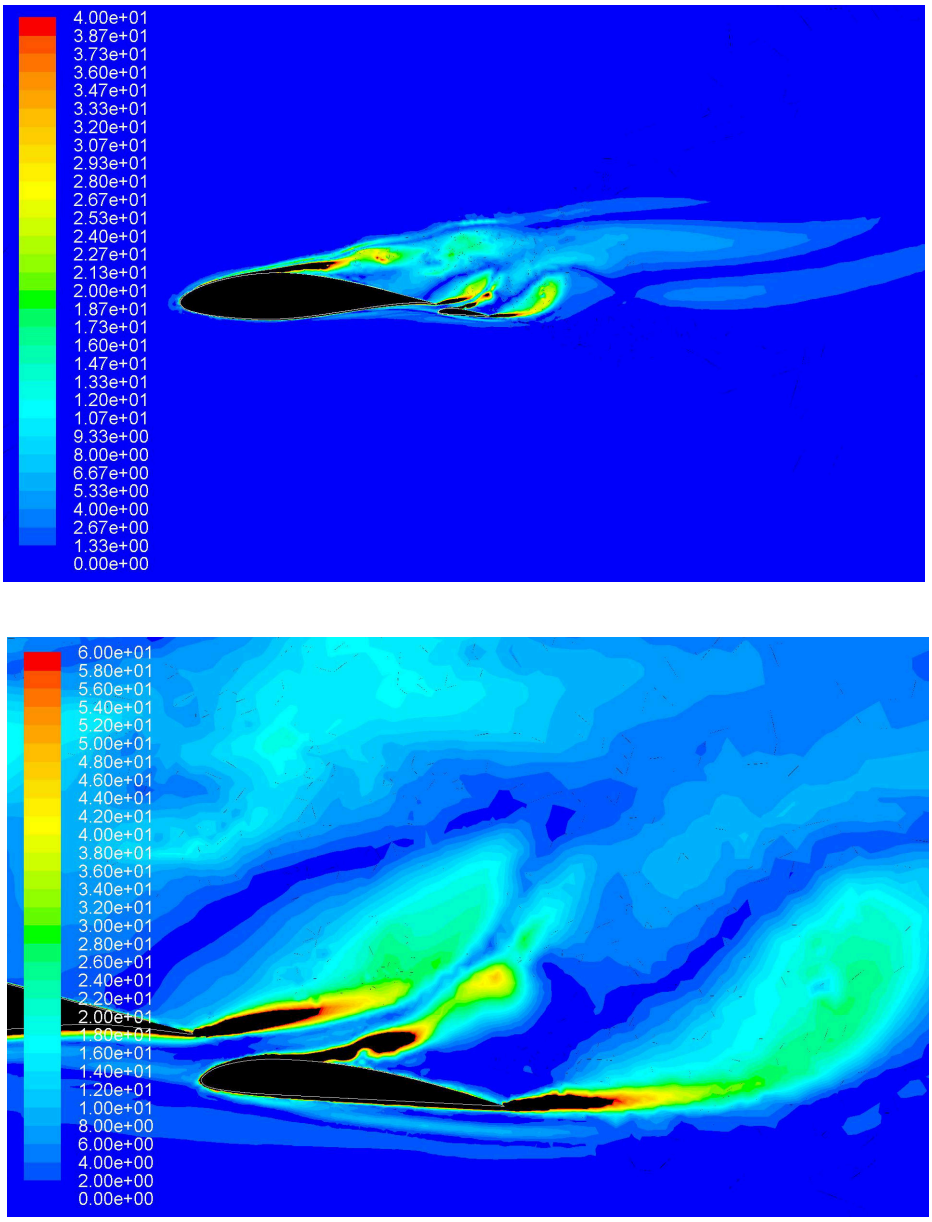

Figure 4.9: Qualitative representation of significant flow features near the trailing edge of flap actuated airfoil configuration of NACA 64_3-618 with Clark Y actuated $+5°$ at angle of attack $\alpha = +16°$. Top panel: Contour plot of vorticity magnitude; Bottom panel: Close-up of the trailing edge.

To illustrate certain aspects of the flow behavior around the airfoil sections and its interaction with the flap, some graphical representations of velocity and vorticity magnitude distributions and flow direction vectors are included for the case of a NACA 64_3-618 / Clark Y

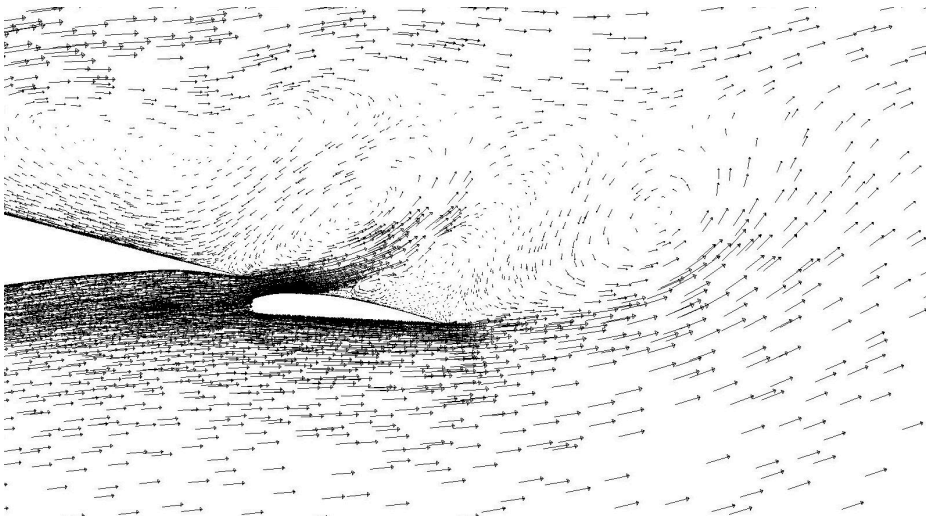

Figure 4.10: Qualitative representation of significant flow features near the trailing edge of flap actuated airfoil configuration of NACA 64_3-618 with Clark Y actuated $+5^\circ$ at angle of attack $\alpha = +16^\circ$. This is a closer view of vector plot of velocity magnitude.

assembly, with the flap actuated at $+5^\circ$, for two angles of attack $\alpha = +8^\circ$ and $\alpha = +16^\circ$, which are representative of the attached and separated flow regimes respectively. The angles of attack were selected to ensure the flow properties shown has noticeable effect on the flow behavior. Figure 4.6 shows the contour plot and vector plot of velocity magnitude near the trailing-edge region of the airfoil with the Clark Y flap actuated at $+5^\circ$. Figure 4.7 depicts the vorticity magnitude around the airfoil in the same configuration, with close attention to the trailing-edge. Note the difference in flow structure as the angle of attack increases to $+16^\circ$ in figure 4.8, which shows the overall velocity magnitude around the airfoil in the same configuration with the flap. Figure 4.9 reinstates the flow characteristics for this configuration with depictions of the vortical behavior. A closer observation of the vortical structures near the trailing edge for this angle of attack is shown in figure 4.10. These graphical depictions are provided for the comprehension of the flow structure around the airfoil and how the trailing-edge flap plays a role in modifying them.

4.2 Study of DU 93-W-210

Airfoil sections such as the DU 93-W-210 were designed for specific use on the inboard span regions of wind turbine blades. They have the unique characteristics of maintaining relatively high aerodynamic efficiency despite the fact that they are inherently designed with supreme structural stability. Trying to reduce the weight of a turbine blade catches the two key aspects of such airfoil sections (structural stability and aerodynamic efficiency) in conflicting paths. As noted in table 4.1, DU 93-W-210 is used on approximately $4.1\ m$ span of the $61.5\ m$ long standard blade used on the NREL-5MW RWT. Unique features have expanded their use on various large wind turbine rotors that are currently in operation, and this airfoil section is also an integral part of other contemporary studies on future wind turbine blade designs [5, 40]. With the primary purpose of augmenting the structural stability of the blade, these airfoils are commonly refereed as semi-thick airfoils and acts as the transition from the *structurally stable* parts to the *aerodynamically active* parts of the turbine blade. Flow-control devices used for these sections could add more functionality be providing more aerodynamic flexibility of operation.

Computational evaluation were carried out for the DU 93-W-210 in various configurations as a two-element airfoil with the trailing-edge flap. The effects of the use of a 20% chord flap with Clark Y profile were assessed in this respect. Location for the flap actuation hinge was obtained from studies conducted on use of high-lift devices on NACA 23012. As a standardization procedure to establish the numerical solution setup, the airfoil in its original configuration was studied without any flow-control devices attached. And the numerical results from this study were validated by a discrete comparison of the coefficients

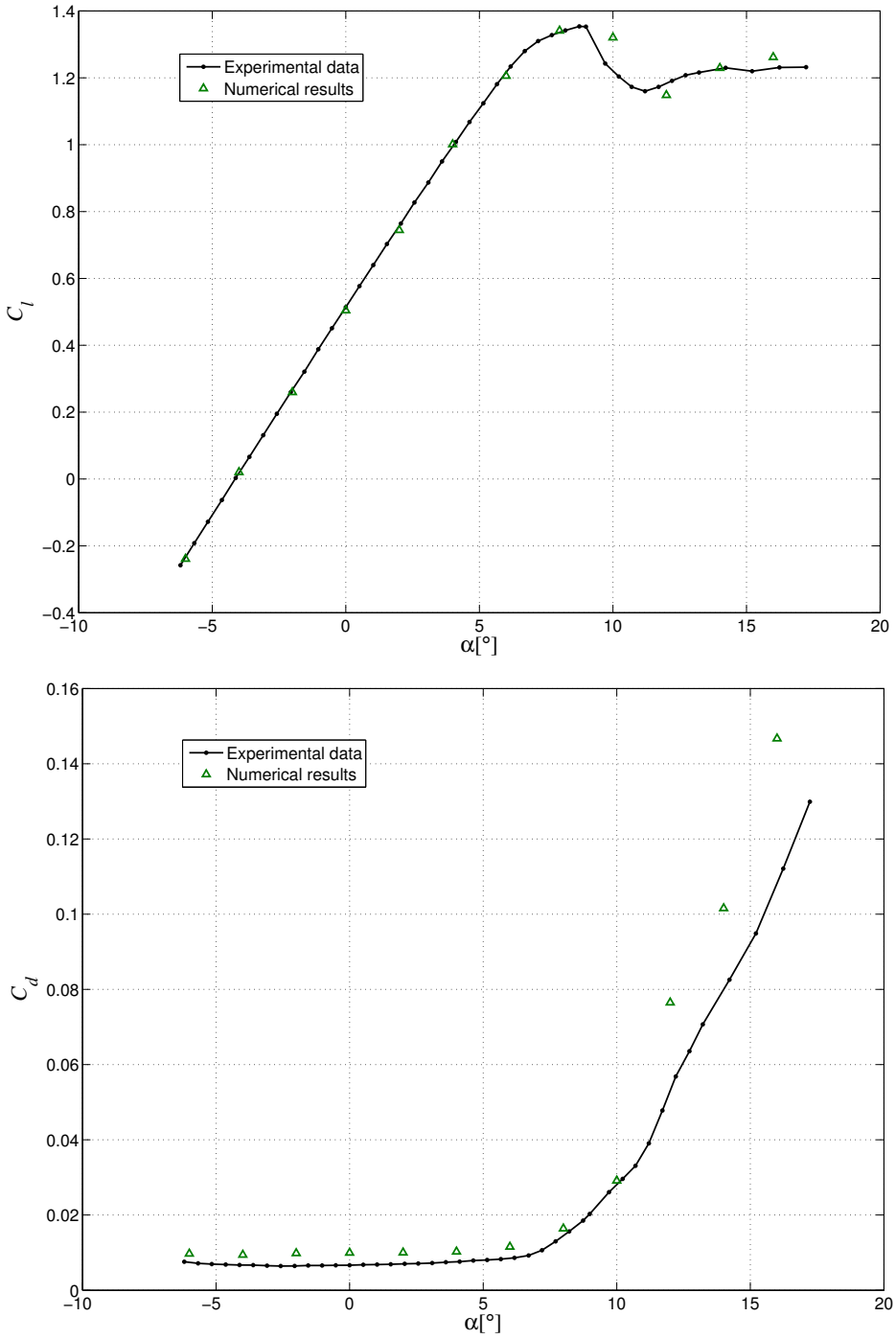

Figure 4.11: Numerical results for aerodynamic coefficients of the DU 93-W-210 airfoil compared with experimental results [4]. Top panel: lift coefficient C_l, bottom panel: drag coefficient C_d, both plotted against angle of attack α.

against the experimental results [4]. Figure 4.11 shows the results of this numerical comparison of results, where the experimental values were obtained from the Delft University of Technology who designed this airfoil section. Numerical simulations were completed in an environment setup with standard air density and modified dynamic viscosity for a flow field normalized by velocity to match a Reynold's number of 3×10^6. The coefficients were computed for a range of angles of attack from -6° to $+26^\circ$, which comprises major operating conditions for the turbine blade regions where the modified sections would be used. The airfoil sections equipped with the flow-control devices were studied for three configurations of the airfoil-flap assembly, with the Clark Y flap actuated at -5°, 0°, and $+5^\circ$. The range of actuation angles of the trailing-edge flap covered in the current study is a modest approach and can be extended to higher actuation angles (both in positive and negative directions), providing more flexibility of operation. As noted before, the most important coefficients characterizing the aerodynamic behavior of airfoil sections are the coefficients of lift, drag, and momentum, which were reported in steps of 2° within the range of angles of attack studied. The discrete values of coefficients reported from the numerical study indicates comparability to the experimental results and hence, shows consistency in numerical approximation for the regime of flow studied. This also justifies the extension of the approach to compute aerodynamic characteristics of DU 93-W-210 equipped with trailing-edge flaps.

To evaluate the characteristics of airfoil-flap assemblies, the numerical approach followed for DU 93-W-210 in its original configuration was extended with slight modifications to incorporate the use of trailing-edge flaps. Coefficients indicators of aerodynamic behavior for the modified airfoil section with the flap actuated at different angles (β) were measured and reported to cover the same range of angles of attack (α). The simulations were run

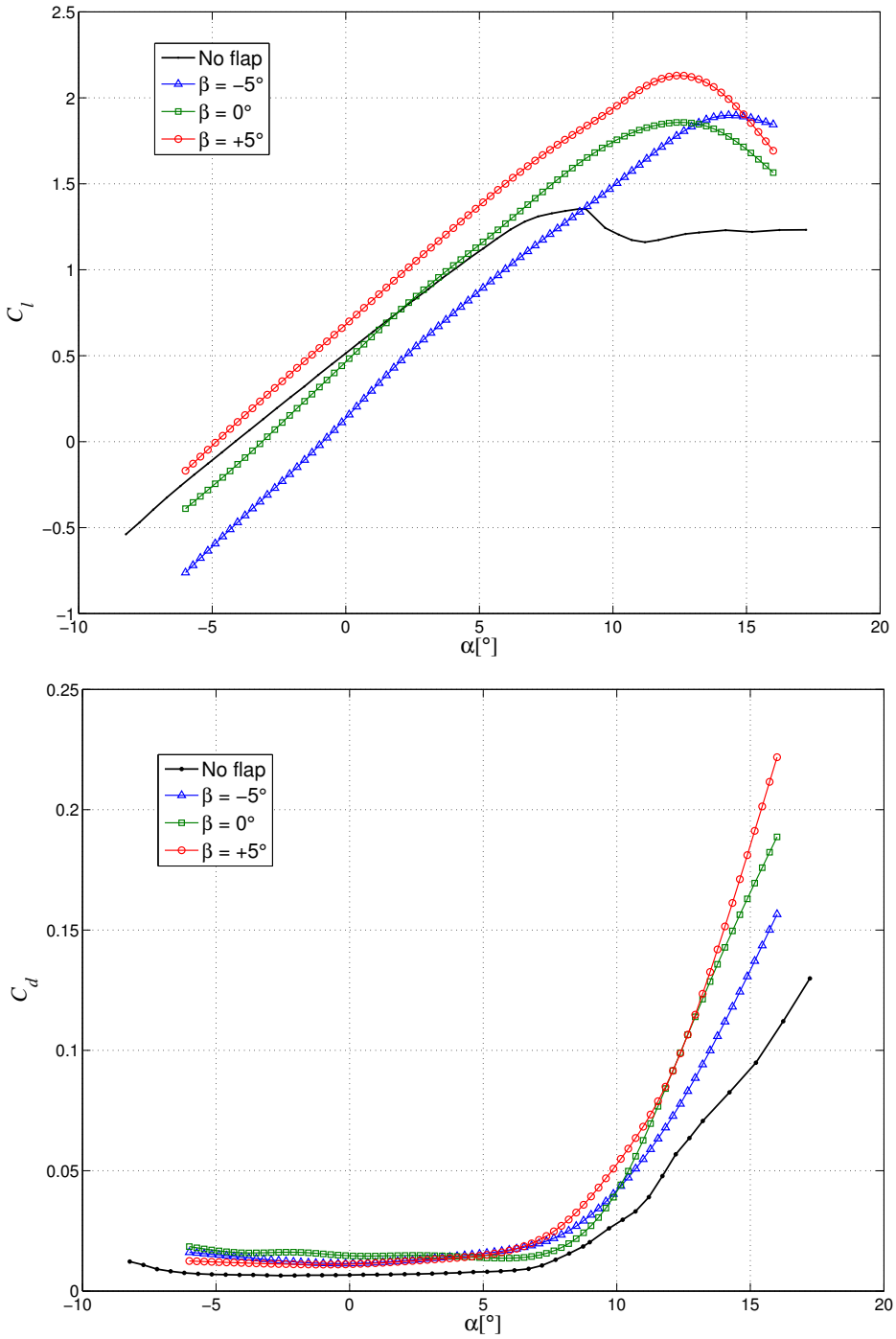

Figure 4.12: Numerical results for aerodynamic coefficients of a DU 93-W-210 airfoil section with trailing-edge flap Clark Y actuated at $-5°$, $0°$, and $+5°$. Experimental data for the 'No flap' configuration are included for reference. Top panel: lift coefficient C_l, bottom panel: drag coefficient C_d, both plotted against angle of attack α.

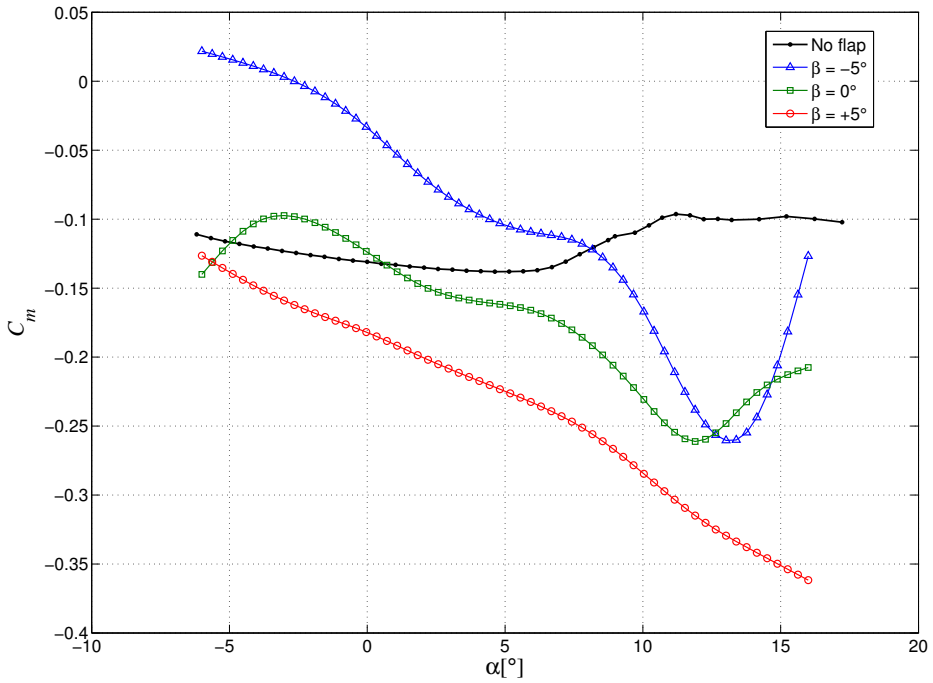

Figure 4.13: Numerical results for aerodynamic coefficients of pitching moment C_m, reported for a DU 93-W-210 airfoil section with trailing-edge flap Clark Y actuated at $-5°$, $0°$, and $+5°$, plotted against angle of attack α. Experimental data for the 'No flap' configuration are included for reference.

in a numerical environment setup in the same manner to obtain a Reynold's number of 3×10^6. The primary indicators of aerodynamic behavior, which are the coefficients of lift, and drag are reported in figure 4.12 for DU 93-W-210 with the Clark Y profile trailing-edge flap actuated at three different angles, $-5°$, $0°$, and $+5°$. They are reported along side the experimental behavior plot (indicated as the 'No flap') for put in perspective the alteration in characteristics brought about by the presence of the flap. Lift and drag forces, which are the most important component in determining the driving torque for the wind turbine operation are directly dependent on these coefficients. The significance of the alteration in the aerodynamic behavior is hence noticeable from the lift and drag plots. The corresponding coefficients of pitching moment for the same configurations are reported in the figure 4.13. These moment coefficients are reported at quarter-chord length from the leading-edge of

the main airfoil, which is a standard procedure in airfoil aerodynamics. That is, for a $1\ m$ long airfoil section it would be reported at $0.25\ m$ from the leading-edge.

The characteristics of the modified airfoil section with the flap actuated at -5° is an important case for a semi-thick airfoil such as the DU 93-W-210, considering the low angles of attack they are subject to during normal operating conditions. The relative wind velocity incident on airfoil sections in the inboard regions of the blade will have a lower angle of attack as a resultant of lower angular speed. A closer observation of angles ranging from -6° to $+6^{\circ}$ in the bottom panel of figure 4.12 indicates a drop in lift behavior in comparison to the 'No flap' configuration. This reduction in the lift generation at low angles of attack is relevant when the flow is attached to the boundary layer on the surface of the multi-element airfoil section, and is explained by gap opening more in a nose down configuration for the flap (i.e. $\beta = -5^{\circ}$). On the other hand, lift generation increases when the trailing-edge flap is actuated at $+5^{\circ}$, which is the result of established low pressure zone near the upper surface. This drop in pressure is the resultant of revitalized high speed flow near the trailing edge as an outcome of the gap reduction in a nose-up orientation of the flap (i.e. $\beta = +5^{\circ}$). Figure 4.12 also suggests a neutral position for the modified section when the flap is actuated at 0°, which retains the lift coefficients near the original values for the 'No flap' configuration throughout the attached regime of flow. Even as a neutral position, this configuration demonstrates the ability to delay the onset of stall, as can be noted by the extension of the lift plot beyond the separation angle of attack for t'No flap' configuration. This allows more control-ability to either increase or decrease the lift by actuating the flap towards nose-up or nose-down orientation respectively and ensures more flexibility of operation for the turbine blade. It is also to be noted that this flexibility in lift behavior are produced with negligible variation in coefficients of drag (see bottom panel of figure 4.12).

However, the proportional drag increments are relatively larger for DU 93-W-210 as compared to for NACA 64_3-618, which is justified for a semi-thick airfoil. At higher angles of attack ($\alpha > +6^\circ$), the flap is consistent to delay the onset of stall and in improving the maximum lift generation, irrespective of the angle of actuation (β). This is again the result of a revitalization of the flow near the trailing edge, which is more evident in the case of a DU 93-W-210. Increase in the maximum lift coefficient extends the range of angles of operation permissible for this airfoil section and hence, widens the scope of operating conditions for the wind turbine.

To illustrate certain aspects of the flow behavior around the airfoil sections and its interaction with the flap, some graphical representations of velocity and vorticity magnitude distributions and flow direction vectors are included for the case of a DU 93-W-210 / Clark Y assembly, with the flap actuated at -5°, 0°, and $+5^\circ$, at an angle of attack $\alpha = +10^\circ$. A close observation of these quantities near the trailing-edge of the airfoil for different configurations indicate the dependence of flow modification on the actuation angle of the flap. Figure 4.14 is a representation of the velocity magnitude near the trailing edge for the airfoil with the attached flap actuated at -5°. The contour and vector plots observed side-by-side gives a better understanding of the flow structure. Figure 4.15 shows the vortical structures around the airfoil, with a closer observation near the trailing-edge where the presence of flap changes the flow significantly. Figure 4.16 is a representation of the velocity magnitude for the airfoil with flap actuated at 0°, and figure 4.17 shows the vortical behavior in the same configuration. Figure 4.18 is a representation of the velocity magnitude in the case of flap actuated at $+5^\circ$, and figure 4.19 shows the vortical behavior in the same configuration. It is interesting to note the difference in the vortical behavior near the trailing-edge with change in actuation angle of the flap. This phenomena plays a key role in modification of

the aerodynamic behavior of the airfoil sections.

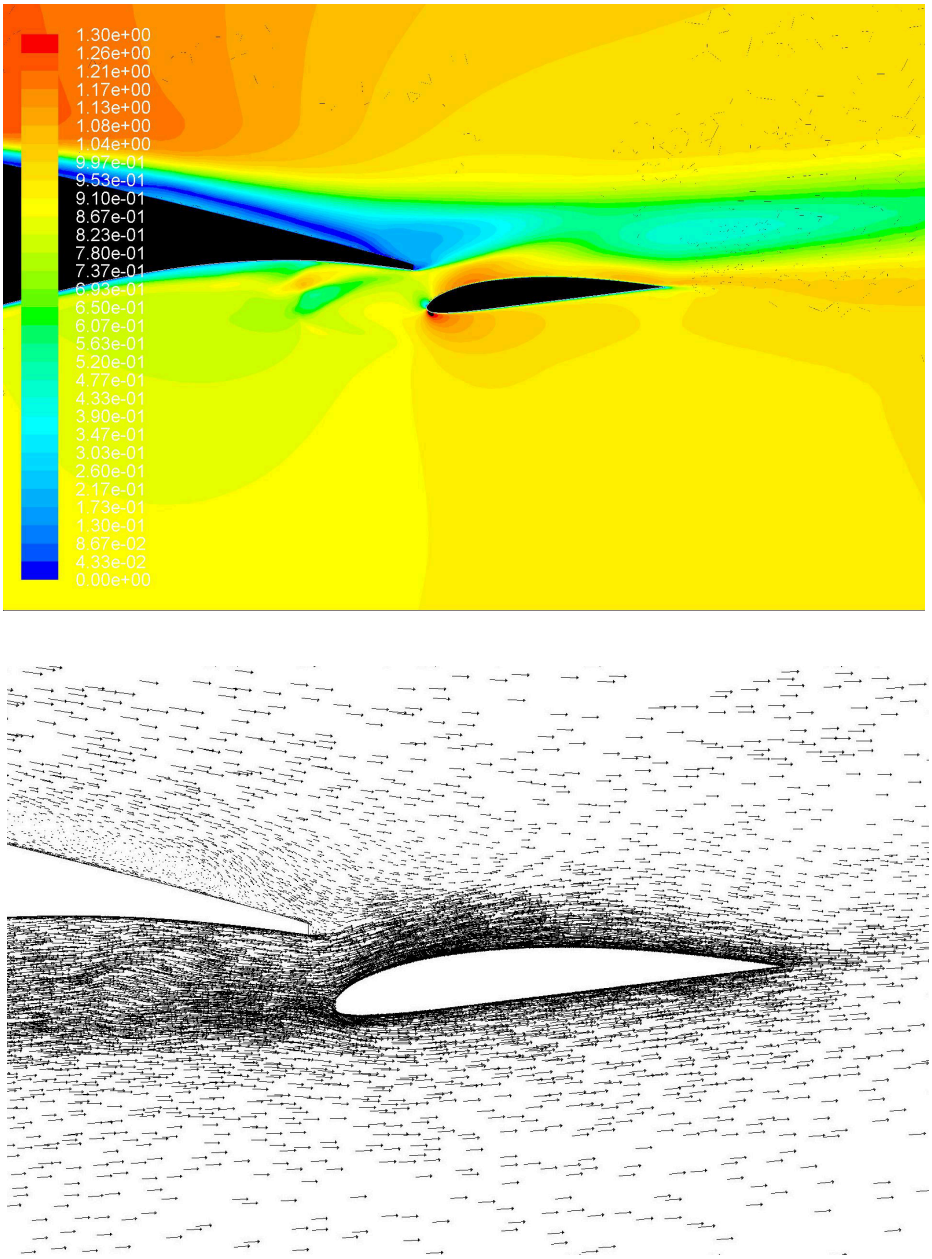

Figure 4.14: Qualitative representation of significant flow features near the trailing edge of flap actuated airfoil configuration of DU 93-W-210 with Clark Y actuated -5° at angle of attack $\alpha = +10^\circ$. Top panel: Contour plot of velocity magnitude; Bottom panel: Vector plot of velocity magnitude.

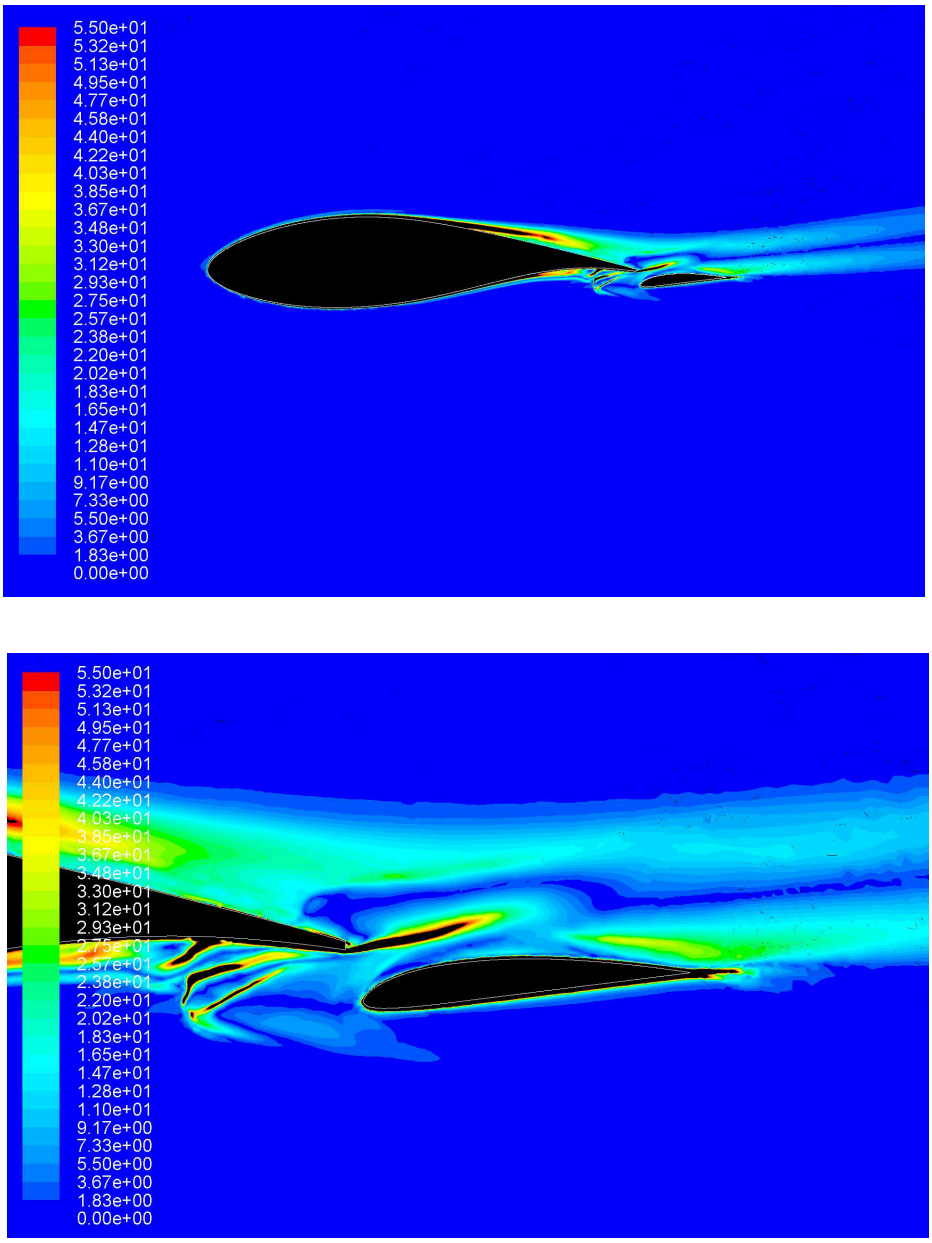

Figure 4.15: Qualitative representation of significant flow features near the trailing edge of flap actuated airfoil configuration of DU 93-W-210 with Clark Y actuated -5° at angle of attack $\alpha = +10^{\circ}$. Top panel: Global view of contour plot of vorticity magnitude; Bottom panel: Closer view .

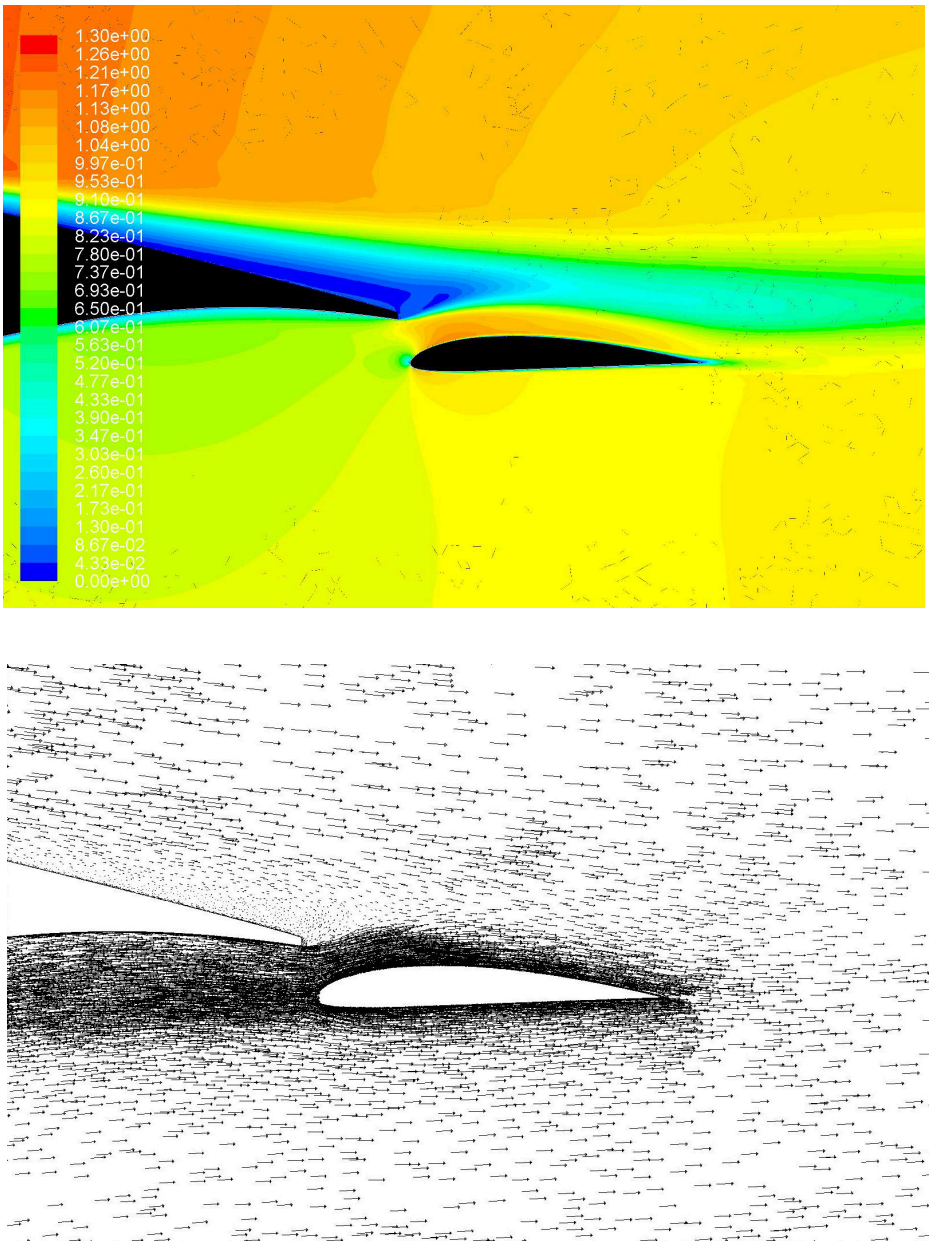

Figure 4.16: Qualitative representation of significant flow features near the trailing edge of flap actuated airfoil configuration of DU 93-W-210 with Clark Y actuated 0° at angle of attack $\alpha = +10^\circ$. Top panel: Contour plot of velocity magnitude; Bottom panel: Vector plot of velocity magnitude.

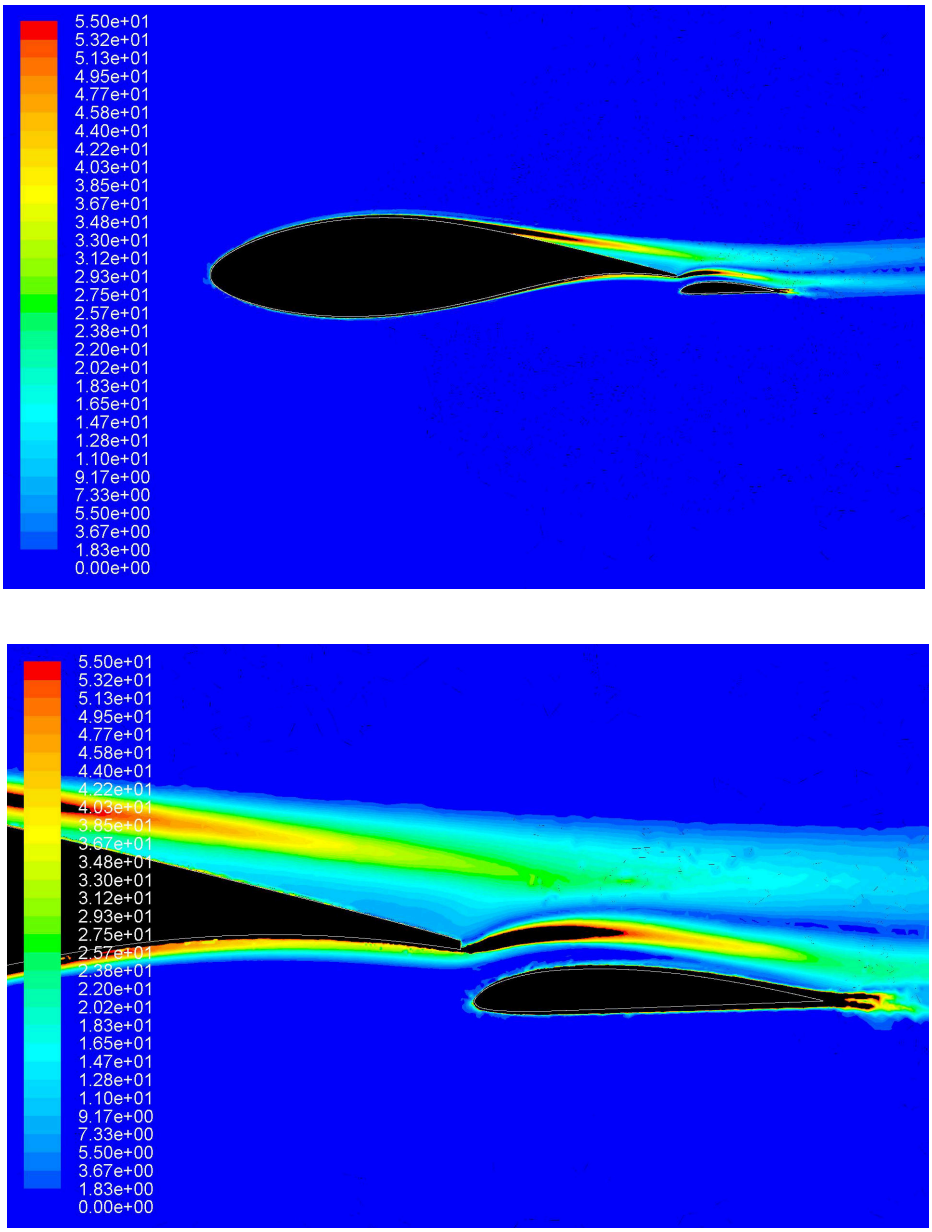

Figure 4.17: Qualitative representation of significant flow features near the trailing edge of flap actuated airfoil configuration of DU 93-W-210 with Clark Y actuated 0° at angle of attack $\alpha = +10^\circ$. Top panel: Global view of contour plot of vorticity magnitude; Bottom panel: Closer view .

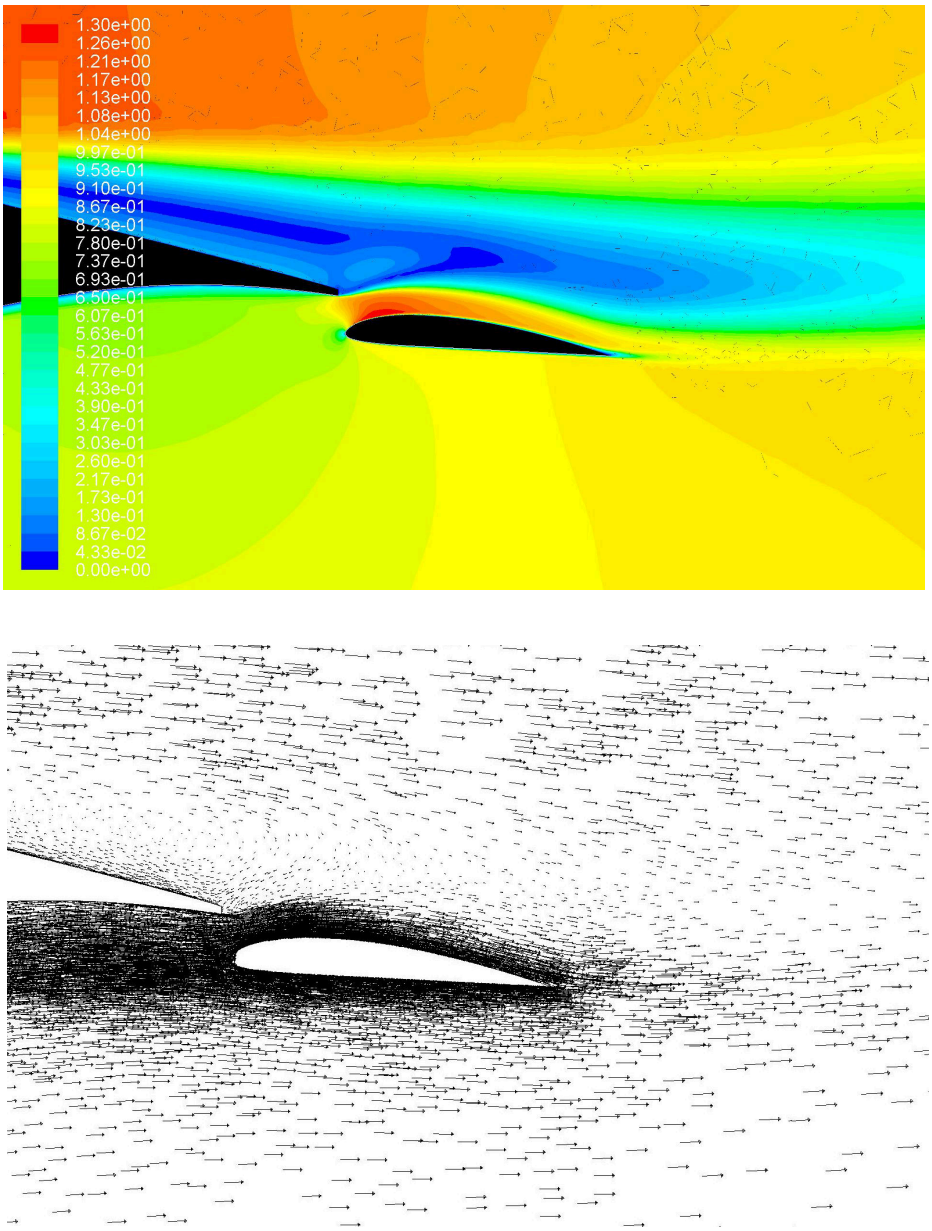

Figure 4.18: Qualitative representation of significant flow features near the trailing edge of flap actuated airfoil configuration of DU 93-W-210 with Clark Y actuated $+5°$ at angle of attack $\alpha = +10°$. Top panel: Contour plot of velocity magnitude; Bottom panel: Vector plot of velocity magnitude.

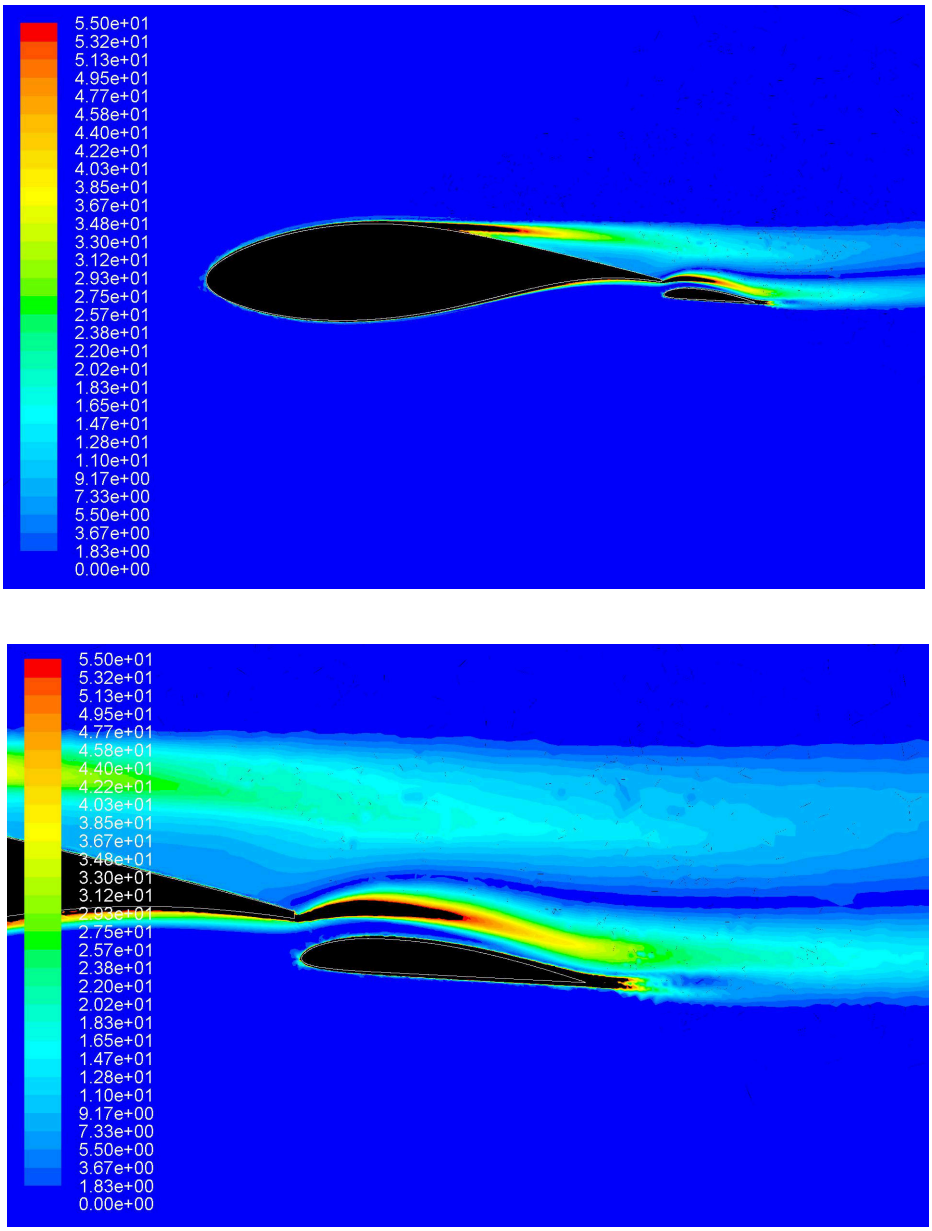

Figure 4.19: Qualitative representation of significant flow features near the trailing edge of flap actuated airfoil configuration of DU 93-W-210 with Clark Y actuated $+5^{\circ}$ at angle of attack $\alpha = +10^{\circ}$. Top panel: Global view of contour plot of vorticity magnitude; Bottom panel: Closer view .

Chapter 5

Conclusion

This dissertation presents results for the aerodynamic properties of airfoil sections specifically intended for wind-turbine applications, when they are appended with trailing-edge slotted flaps. Featuring them as modular devices, these devices can be attached to existing blade designs and could present an innovative approach to formulate load-mitigation strategies in wind turbine operation. As modular attachments, they present a cost-effective active control methodology with minimal alteration to blade manufacturing processes along with offering comparable aerodynamic efficiency. The slotted-flap concept proves to continuously promote a delay in the incipient separation through flow modifications near the trailing edge. This revitalization of boundary layer on the upper surface of blade sections by reattachment of separated boundary layer makes these flaps attractive for use as flow-control devices on such airfoil sections.

The numerical approach in computation of these properties was standardized through validation for a two-element airfoil-flap assembly using NACA 23012 as the main airfoil and

a fractional-chord flap of Clark Y profile. Along with this, an optimum position for the flap actuation hinge as recommended by Platt [2] was used to implement the Clark Y flap on two typical airfoils used in wind turbine applications. These two airfoil sections, NACA 64_3-618 and DU 93-W-210 are classic examples of airfoils used in the external span section of blades for modern wind turbines such as the NREL-5MW RWT that could be considered as a well-established reference for state-of-the-art wind turbine blades. Located in the outboard region of the blade, these two airfoils cover a great extend of the span which contributes most to the aerodynamic forces for the turbine (i.e. the *aerodynamically active* part of the blade). The numerical computations present the aerodynamic coefficients of these two sections when attached with a Clark Y flap and actuated at various angles. This serves as valuable data for the design of future innovative turbine blades with active flow-control devices. These faster time response devices consuming low actuation-energy offers effective alternatives for designing turbine blades operating safely in a wide range of wind conditions.

Aerodynamic efficiency is one of the most important factors in selecting airfoil sections for any blade design. An understanding of the variation in efficiency is hence imminent in introducing design alterations to airfoil sections. An external flap attachment near the trailing-edge increases the chord length by 20% which qualitatively increases both the lift and drag as a result of the larger surface area per unit span. As a result, there is reduction in efficiency for the two-dimensional airfoil section, which is expected with any modification to an original airfoil design. Despite the two-dimensional detrimental effects, using these devices on wind turbine blades have advantages significant in a more global perspective. Use on relatively smaller span sections ensures preserving original configuration for most sections and hence retaining the original aerodynamic efficiency of the blade in its entirety.

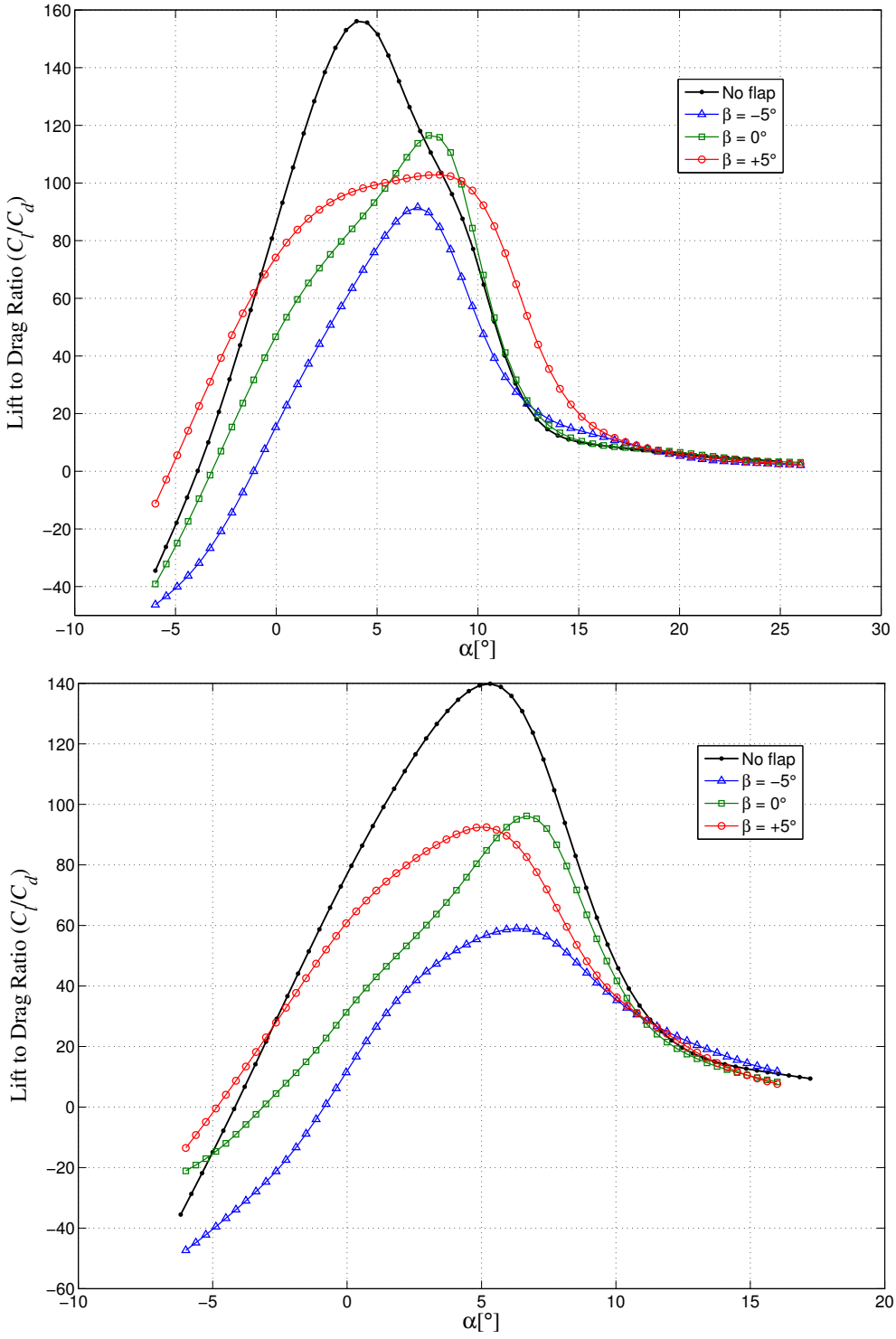

Figure 5.1: Numerical results of lift-to-drag ratio for airfoil sections with Clark Y flap actuated at $-5°$, $0°$, and $+5°$. Top panel: NACA 64_3-618, bottom panel: DU 93-W-210. The 'No flap' configurations are provided for reference.

Reporting the lift-to-drag ratio for NACA 64_3-618 and DU 93-W-210 in their modified configuration, figure 5.1 illustrates that the efficiency deficit is not significant compared to the 'No flap' configuration. This ratio is a great indicator of the efficiency of the modified airfoil sections and shows dependency on the angle of actuation of the flap. They also provide an indication of which are the ranges of actuation more convenient in terms of aerodynamic efficiency, helping to design an optimum control strategy. The trailing-edge flaps provide more flexibility of operation through control on lift for higher torque generation at certain angles of flap actuation β, with other angles acting as power-limitation of load-mitigation configurations.

The results reported in this dissertation form a repository of new aerodynamic properties for modified airfoil sections relevant to wind power applications (using trailing-edge flaps), which in itself could form building blocks for future studies on innovative blade designs and use of other flow-control devices. As an outlook for further work, this data can be integrated into a model platform for the aeroelastic study of wind turbine rotors [29, 46, 47] for a complete analysis of wind turbine rotor dynamics with the eventual objective of designing innovative wind turbine blades based on actively controlled modular-flap devices.

References

[1] Fichaux, N., Beurskens, J., Jensen, P.H., Wilkes, J., Frandsen, S., Sorensen, J., et al. Upwind: Design limits and solutions for very large wind turbines. Sixth Framework Programme 2011;.

[2] Platt, R.C.. Aerodynamic characteristics of wings with cambered external–airfoil flaps including lateral control with a full–span flap. Report NACA–TR–541; National Advisory Committee for Aeronautics. Langley Aeronautical Lab, Langley Field VA, United States; 1936.

[3] Abbott, I.H., Doenhoff, A.E.V.. Theory Of Wing Sections: Including A Summary Of Airfoil Data. Dover Publications; 1959.

[4] Timmer, W.A., van Rooij, R.P.J.O.M.. Summary of the Delft University wind turbine dedicated airfoils. In: 41st Aerospace Sciences Meeting and Exhibit. Reno, Nevada: AIAA; 2003,.

[5] Kooijman, H.J.T., Lindenburg, C., Winkelaar, D., van der Hooft, E.L.. Dowec 6 MW pre-design. Tech. Rep.; ECN-CX-01-135, Energy Research Center of the Netherlands, Petten; 2003.

[6] Vestas, . Capacity of v164 offshore turbine increased to 8 mw. 2012. (accessed Jan 2015); URL http://vestas.com/en/investor/~/media/c57ee170a4fb4266893298875d94ee32.ashx.

[7] Manwell, J.F., McGowan, J.G., Rogers, A.L.. Wind energy explained: Theory, design and application. Chichester, UK: Wiley; 2002.

[8] Bak, C., Bitsche, R., Yde, A., Kim, T., Hansen, M.H., Zahle, F., et al. Light rotor: The 10-mw reference wind turbine. In: EWEA 2012-European Wind Energy Conference & Exhibition. 2012,.

[9] Stuart, J.G., Wright, A.D., Butterfield, C.P.. Wind turbine control systems: dynamic model development using system identification and the FAST structural dynamics code. National Renewable Energy Laboratory; 1996.

[10] Barlas, T.K., Van Kuik, G.. State of the art and prospectives of smart rotor control for wind turbines. In: Journal of Physics: Conference Series; vol. 75. IOP Publishing; 2007, p. 012080.

[11] Van Wingerden, J., Hulskamp, A., Barlas, T., Marrant, B., Van Kuik, G., Molenaar, D.P., et al. On the proof of concept of a 'smart'wind turbine rotor blade for load alleviation. Wind Energy 2008;11(3):265–280.

[12] Bianchi, F.D., De Battista, H., Mantz, R.J.. Wind turbine control systems: principles, modelling and gain scheduling design. Springer Science & Business Media; 2006.

[13] Muljadi, E., Pierce, K., Migliore, P.. Control strategy for variable-speed, stall-regulated wind turbines. In: American Control Conference, 1998. Proceedings of the 1998; vol. 3. IEEE; 1998, p. 1710–1714.

[14] Muljadi, E., Butterfield, C.P.. Pitch-controlled variable-speed wind turbine generation. Industry Applications, IEEE Transactions on 2001;37(1):240–246.

[15] Herrera, J., Reddoch, T., Lawler, J.. Harmonics generated by two variable speed wind generating systems. Energy Conversion, IEEE Transactions on 1988;3(2):267–273.

[16] Steinbuch, M.. Optimal multivariable control of a wind turbine with variable speed. Wind Engineering 1987;11(3):153–163.

[17] Bossanyi, E.. Further load reductions with individual pitch control. Wind energy 2005;8(4):481–485.

[18] Larsen, T.J., Madsen, H.A., Thomsen, K.. Active load reduction using individual pitch, based on local blade flow measurements. Wind Energy 2005;8(1):67–80.

[19] Polinder, H., Bang, D., van Rooij, R., McDonald, A., Mueller, M.. 10 mw wind turbine direct-drive generator design with pitch or active speed stall control. In: Electric Machines & Drives Conference, 2007. IEMDC'07. IEEE International; vol. 2. IEEE; 2007, p. 1390–1395.

[20] Salameh, Z.. Operation of the variable speed constant frequency double output induction generator (vscf-doig) in a constant optimum power coefficient mode. Wind Engineering 1985;9:67–75.

[21] Hohenemser, K., Swift, A.. On the design of horizontal axis two-bladed hinged wind turbines. Journal of solar energy engineering 1984;106(2):171–176.

[22] Lobitz, D.W., Veers, P.S.. Load mitigation with bending/twist-coupled blades on rotors using modern control strategies. Wind Energy 2003;6(2):105–117.

[23] Johnson, S.J., Baker, J.P., Van Dam, C., Berg, D.. An overview of active load control techniques for wind turbines with an emphasis on microtabs. Wind Energy 2010;13(2-3):239–253.

[24] Zayas, J., van Dam, C., Chow, R., Baker, J., Mayda, E.. Active aerodynamic load control for wind turbine blades. In: European Wind Energy Conference. Athens, Greece; 2006,.

[25] Van Dam, C., Berg, D.E., Johnson, S.J.. Active load control techniques for wind turbines. Tech. Rep. SAND2008-4809; Sandia National Laboratories; 2008.

[26] Muljadi, E., Pierce, K.G., Migliore, P.G.. A conservative control strategy for variable-speed stall-regulated wind turbines. National Renewable Energy Laboratory; 2000.

[27] Ponta, F.L., Otero, A.D., Rajan, A., Lago, L.I.. The adaptive-blade concept in wind-power applications. Energy for Sustainable Development 2014;22(0):3 – 12. doi:\bibinfo{doi}{http://dx.doi.org/10.1016/j.esd.2014.04.004}. Wind Power Special Issue.

[28] Griffin, D.A.. Evaluation of design concepts for adaptive wind turbine blades. Report SAND2002-2424; Sandia National Laboratories; 2002.

[29] Lago, L.I., Ponta, F.L., Otero, A.D.. Analysis of alternative adaptive geometrical configurations for the NREL-5 MW wind turbine blade. Renewable Energy 2013;59:13 – 22. doi:\bibinfo{doi}{http://dx.doi.org/10.1016/j.renene.2013.03.007}. URL http://www.sciencedirect.com/science/article/pii/S0960148113001638.

[30] Kooijman, H.. Bending-torsion coupling of a wind turbine rotor blade. Netherlands Energy Research Foundation ECN; 1996.

[31] Sadraey, M.H.. Aircraft design: A systems engineering approach. John Wiley & Sons; 2012.

[32] Young, A.D.. The aerodynamic characteristics of flaps. Tech. Rep.; DTIC Document; 1947.

[33] Weyl, A.. High-lift devices and tailless aeroplanes. Aircraft Engineering and Aerospace Technology 1945;17(10):292–297.

[34] Rogers, S.E.. Progress in high-lift aerodynamic calculations. Journal of Aircraft 1994;31(6):1244–1251.

[35] Platt, R.C., Abbott, I.H.. Aerodynamic Characteristics of NACA 23012 and 23021 Airfoils with 20-percent-chord External-airfoil Flaps of NACA 23012 Section. Defense Technical Information Center; 1936.

[36] Platt, R.C., Shortal, J.A.. Wind-Tunnel Investigation of Wings with Ordinary Ailerons and Full-Span External-Airfoil Flaps. National Advisory Committee for Aeronautics; 1937.

[37] Enenkl, B., Klöppel, V., Preißler, D., Jänker, P.. Full scale rotor with piezoelectric actuated blade flaps. In: 28th European Rotorcraft Forum. 2002, p. 17–19.

[38] Narsipur, S., Pomeroy, B., Selig, M.. CFD analysis of multielement airfoils for wind turbines. In: Proceedings of the 30th AIAA Applied Aerodynamics Conference. 2012,.

[39] Cahill, J.F.. Summary of section data on trailing-edge high-lift devices. Tech. Rep. NACA-TR-938; National Advisory Committee for Aeronautics(NACA); 1949.

[40] Jonkman, J., Butterfield, S., Musial, W., Scott, G.. Definition of a 5-MW reference wind turbine for offshore system development. Tech. Rep. NREL/TP-500-38060; National Renewable Energy Laboratory; 2009.

[41] Wilcox, D.C., et al. Turbulence modeling for CFD; vol. 2. DCW industries La Canada, CA; 1998.

[42] Launder, B.E., Spalding, D.. The numerical computation of turbulent flows. Computer methods in applied mechanics and engineering 1974;3(2):269–289.

[43] Wilcox, D.. A half century historical review of the k-omega model. In: 29th Aerospace Sciences Meeting, Reno, US., Report. AIAA; 1991, p. 91–615.

[44] Menter, F.R.. Zonal two equation k-turbulence models for aerodynamic flows. AIAA paper 1993;2906:1993.

[45] Menter, F.R.. Two-equation eddy-viscosity turbulence models for engineering applications. AIAA journal 1994;32(8):1598–1605.

[46] Otero, A.D., Ponta, F.L.. Structural analysis of wind-turbine blades by a generalized Timoshenko beam model. Journal of Solar Energy Engineering 2010;132(1):011015 (pages 8). doi:\bibinfo{doi}{10.1115/1.4000596}.

[47] Ponta, F.L., Otero, A.D., Lago, L.I., Rajan, A.. Effects of rotor deformation in wind-turbine performance: The dynamic rotor deformation blade element momentum model (drd–bem). Renewable Energy 2016;92:157–170.

Appendix A

Copyright Agreements

Copyright statement for figure 1.2, from European Wind Energy Association (EWEA):

- The text, images, video files and audio files that are represented on this site can be reproduced provided data integrity is maintained and EWEA copyright duly indicated.

Attribution:

◇ Figure 1.2 was reproduced from a project report published in collaboration with EWEA by Fichaux et al. [1], © European Wind Energy Association.